

KfK 4763
Januar 1991

Muon Catalyzed Fusion under Compressive Conditions

G. Cripps, B. Goel, A. A. Harms
Institut für Neutronenphysik und Reaktortechnik

Kernforschungszentrum Karlsruhe

KERNFORSCHUNGSZENTRUM KARLSRUHE
Institut für Neutronenphysik und Reaktortechnik

KfK 4763

***Muon Catalyzed Fusion
under Compressive Conditions***

by

G. Cripps** , B. Goel and A.A. Harms*

Kernforschungszentrum Karlsruhe GmbH, Karlsruhe

* Dept. of Engineering Physics, McMaster University, Hamilton, Canada

** on leave from

Dept. of Engineering Physics, McMaster University, Hamilton, Canada

Als Manuskript gedruckt
Für diesen Bericht behalten wir uns alle Rechte vor

Kernforschungszentrum Karlsruhe GmbH
Postfach 3640, 7500 Karlsruhe 1

ISSN 0303-4003

Abstract

The viability of a symbiotic combination of Muon Catalyzed Fusion (μ CF) and high density generation processes has been investigated. The muon catalyzed fusion reaction rates are formulated in the temperature and density range found under moderate compressive conditions. Simplified energy gain and power balance calculations indicate that significant energy gain occurs only if standard type deuterium-tritium (dt) fusion is ignited. A computer simulation of the hydrodynamics and fusion kinetics of a spherical deuterium-tritium pellet implosion including muons is performed. Using the muon catalyzed fusion reaction rates formulated and under ideal conditions, the pellet ignites (and thus has a significant energy gain) only if the initial muon concentration is approximately 10^{17} cm^{-3} . The muons need to be delivered to the pellet within a very short time ($\sim 1 \text{ ns}$). The muon pulse required in order to make the high density and temperature muon catalyzed fusion scheme viable is beyond the present technology for muon production.

Müonen-katalysierte Fusion für verdichtete Zustände

Die Machbarkeit einer Symbiose der Müonen-katalysierten Fusion mit Verdichtungs Vorgängen wurde untersucht. Die Reaktionsraten der Müonen-katalysierten Fusionsprozesse für die Temperaturen und Dichten, die bei mäßiger Verdichtung vorkommen, wurden formuliert. Vereinfachte Berechnungen zeigen, daß signifikanter Energiegewinn nur dann zu beobachten ist, wenn der Deuterium-Tritium Brennstoff in herkömmlicher Weise zur Fusionszündung gebracht wird. Simulationen der hydrodynamischen und fusionskinetischen Prozesse einschließlich der Müonen-katalysierten Fusion wurden für ein sphärisches Deuterium-Tritium Pellet durchgeführt. Unter idealisierten Bedingungen wird das Pellet nur bei einer Müonen-Konzentration von 10^{17} cm^{-3} gezündet. Die Müonen sollen in sehr kurzer Zeit ($\sim 1 \text{ ns}$) bereitgestellt werden. Diese hohe Müonen-Konzentration ist außerhalb der derzeitigen Technologie.

Table of Contents	Page
1. Introduction	1
2. Muon Catalyzed Fusion Concepts	3
2.1 Muons in deuterium-tritium	3
2.2 Ionization and dissociation of hydrogen	4
2.2.1 Ionization model	4
2.2.2 Dissociation model	5
2.2.3 Ionization and dissociation fractions of hydrogen	6
2.3 Muon stopping	6
2.4 Muon capture	7
2.5 Muon transfer	11
2.6 Muo-molecular formation	12
2.6.1 Resonant formation	15
2.6.2 Non-resonant formation (electron emission)	15
2.6.3 Direct radiative capture	17
2.6.4 Dissociative formation	18
2.6.5 Three body reactions	18
2.7 Nuclear fusion	19
2.8 Muon sticking	20
2.9 Kinetics	25
3. Energy Gain Calculations	35
3.1 E_{out}	35
3.2 E_{in}	36
3.3 Energy gain dominated by muon catalyzed fusion	37
3.4 Ignition of standard fusion	39

Table of Contents (cont.)	Page
4. Power Balance Calculations	43
5. Muon Catalyzed Fusion under Compression	51
6. Discussion	61
7. References	63
Appendix A : KATACO with Muon Catalyzed Fusion	65

1. Introduction

The history and feasibility of cold nuclear fusion using muons is well documented (1,2,3). Current estimates conclude that a fusion reactor based on muon catalyzed fusion at low temperatures ($< 5000^{\circ}\text{C}$) and liquid hydrogen density (LHD) would only be viable if fission fuel breeding is included (4). Some recent experiments have shown that the important reaction parameters (e.g. muo-molecule formation, muon sticking) may increase the muon catalyzed fusion reaction rate at high fuel densities and temperatures (5). It has been suggested that a symbiotic relationship between Muon Catalyzed Fusion (μCF) and a high density generation process such as Inertial Confinement Fusion (ICF) may provide a positive energy gain (6). This novel scheme is most likely to succeed under the following ideal conditions: 50% - deuterium, 50% - tritium fuel (this is the most efficient muon catalyzed fusion and standard fusion fuel) and spherical fuel geometry (this requires the least power to compress the fuel). The key points and issues of the symbiotic relationship are analysed in this idealized scenario and presented in this report.

2. Muon Catalyzed Fusion Concepts

2.1 Muons in deuterium-tritium

In muon catalyzed fusion of deuterium-tritium, nuclear fusion is enabled by 'muon confinement' of deuterium and tritium in a muo-molecular ion. The muon has a mass about 207 times the mass of an electron and therefore the muonic orbit is correspondingly 207 times smaller than the electron's orbit. When a deuteron (d) and a triton (t) are 'circled' by a muon they come close enough that tunneling through the Coulomb barrier is very probable and very fast. The processes leading to the formation of the muo-molecular ion, μdt^+ , can be grouped in the following manner:

1. Slowing down of injected muons,
2. Capture of muons by deuterium or tritium,
3. Isotopic transfer of muons,
4. Muo-molecule formation,
5. Nuclear fusion and release of muon for further catalysis.

Each of these processes will be analyzed in detail for the temperature and density range found in moderate compressive conditions, i.e.: temperatures from 20°K or $\sim 10^{-3}$ eV (cyrogenic hydrogen) to greater than 10⁹°K or 10⁴ eV, and densities with respect to LHD varying from 1 to 1000.

Most of the muon catalyzed fusion processes depend upon the dissociative and ionization state of hydrogen. Therefore a simulation of ionization and dissociation is important and will be discussed first.

Herein only 50-50 deuterium-tritium fuel will be considered. A special problem arises when one speaks of deuterium-tritium mixtures as fuel due to the following exchange reaction,



For cyrogenic fuel this is not a problem since this reaction will not proceed quickly for frozen fuel, however at higher temperatures the concentration of D₂, DT, and T₂ will equalibrate to a ratio of 1:2:1. But the reaction rate for these processes is slower than the compression rate, thereby justifying it's exclusion.

2.2 Ionization and dissociation of hydrogen

There are many possible reaction mechanisms of ionization and dissociation in molecular hydrogen when one considers all possible interactions. In order to greatly simplify the dynamics of ionization and dissociation only the following dominant reactions are considered (7).



Reaction 2.2 shows the hydrogen molecule dissociation and Reaction 2.3 shows the atomic hydrogen ionization. The dissociative and ionization properties for the heavy isotopic combinations of hydrogen (D_2 , T_2) are not significantly different from normal hydrogen, therefore simulation of hydrogen only can be used.

2.2.1 Ionization model

It is difficult to calculate the ionization fraction (the fraction of atoms which are ionized) with a high degree of accuracy at the temperatures and densities of interest here. The normal Saha equation is satisfactory for calculating the ionization fraction for densities (with respect to LHD) less than 1 but breaks down at higher densities (8). As atoms get closer together (when density increases) the atomic spacing becomes smaller than the atomic orbits so ionization occurs at progressively lower energies. Therefore as the density increases, total ionization occurs at lower temperatures. The terms I_{i^*} and $\Phi(r_o)$ in the modified Saha equation include pressure effects necessary to simulate ionization at high densities (8). The modified Saha equation for hydrogen is

$$\frac{\alpha_i^2}{1 - \alpha_i} = 0.142 T_{\text{eV}}^{3/2} \frac{e^{-\frac{I_{i^*}}{T_{\text{eV}}}}}{\phi \Phi(r_o)} \quad [\text{E2.1}]$$

with

α_i as the ionization fraction ,

T_{eV} as the temperature in eV and

ϕ as the density with respect to LHD .

In Equation 2.1

$$I_{i*} = \frac{I_i}{1 + 0.045 \phi^{2/3} + 0.170 \phi} \quad \text{and} \quad [\text{E2.2}]$$

$$\Phi(r_o) = e^{-\left(\frac{a_o}{r_o}\right)^3}, \quad [\text{E2.3}]$$

In the above expressions, I_i is the ionization energy in eV and equals 13.6 eV for hydrogen, a_o is the Bohr radius and equals 5.29×10^{-9} cm and r_o represents the mean distance between hydrogen atoms.

Using the ion sphere model (9), the mean distance between hydrogen atoms is

$$r_o = \left(\frac{3}{4\pi N_o \phi}\right)^{1/3} = 1.78 \times 10^{-8} \phi^{-1/3} \text{ cm} \quad [\text{E2.4}]$$

using $N_o = 4.25 \times 10^{22} \text{ cm}^{-3}$.

2.2.2 Dissociation model

The pressure effect upon the dissociating hydrogen is not as clear as for ionization. Intuitively there should be some similarity. The dissociation fraction was estimated by modifying the Saha equation for dissociation (10) assuming similar pressure effects as those in the modified equation for ionization (see Equation 2.1). This assumption is conservative and at worst will underestimate the dissociation fraction at high pressures. The modified Saha equation for dissociation is

$$\frac{\alpha_d^2}{1 - \alpha_d} = 16 \frac{e^{-\frac{I_{d*}}{T_{eV}}}}{T_{eV}^{1/2} \phi \Phi(r_o)} \quad [\text{E2.5}]$$

with

α_d as the dissociation fraction ,

T_{eV} as the temperature in eV and

ϕ as the density with respect to LHD .

In Equation 2.5

$$I_{d*} \sim I_d \frac{1}{1 + 0.1 \phi} \quad \text{and} \quad [\text{E2.6}]$$

$$\Phi(r_o) = e^{-\left(\frac{d_o}{r_o}\right)^3}. \quad [\text{E2.7}]$$

In the above expressions I_d is the dissociation energy of H_2 which equals 4.5 eV, d_o is the H_2 bond length which equals 0.74×10^{-8} cm and the interatomic distance r_o equals $1.78 \times 10^{-8} \phi^{-1/3}$ cm .

2.2.3 Ionization and dissociation fractions of hydrogen

The fraction of hydrogen left un-ionized, referred to as the ionization fraction, is simply

$$f_i = 1 - \alpha_i . \quad [E2.8]$$

However the fraction left undissociated, referred to as the dissociation fraction, must include ionization and therefore is

$$f_d = 1 - \alpha_d - \alpha_i + \alpha_i \alpha_d . \quad [E2.9]$$

Figure 1A is a plot of the ionization fraction of hydrogen f_i , versus temperature for various densities ($\phi = 1, 5, 10, 50, 100, 500, 1000$). Similarly, Figure 1B shows the dissociation fraction f_d , versus temperature for various densities. (Note: The dissociation fraction is zero for all temperatures at $\phi = 1000$).

The rate of dissociation and ionization are very fast and are always greater than 10^{12} s^{-1} (10). Since these rates are anticipated to be very much faster than any other process, it is possible to decouple the ionization and dissociation dynamics from the other reactions.

2.3 Muon stopping

Muons must be stopped in the fusion fuel (i.e. 50-50 d-t). Muons from a muon synthesizer will have a typical kinetic energy between 0.5 and 1.0 GeV (11). Using an energy deposition simulation program, EDEPOS (12), and inputting constants for muon bombardment of 50-50 d-t mixture at LHD it was found that the range of the 0.5 - 1.0 GeV muons is between 5 and 10 cm (see Figure 2). For a 1 cm sphere (which will be considered in this report) only one tenth of the muons in a beam are stopped. The time for the muon slowing down process even from the highest energy to near thermal energies is very fast, typically in the nanosecond range (13).

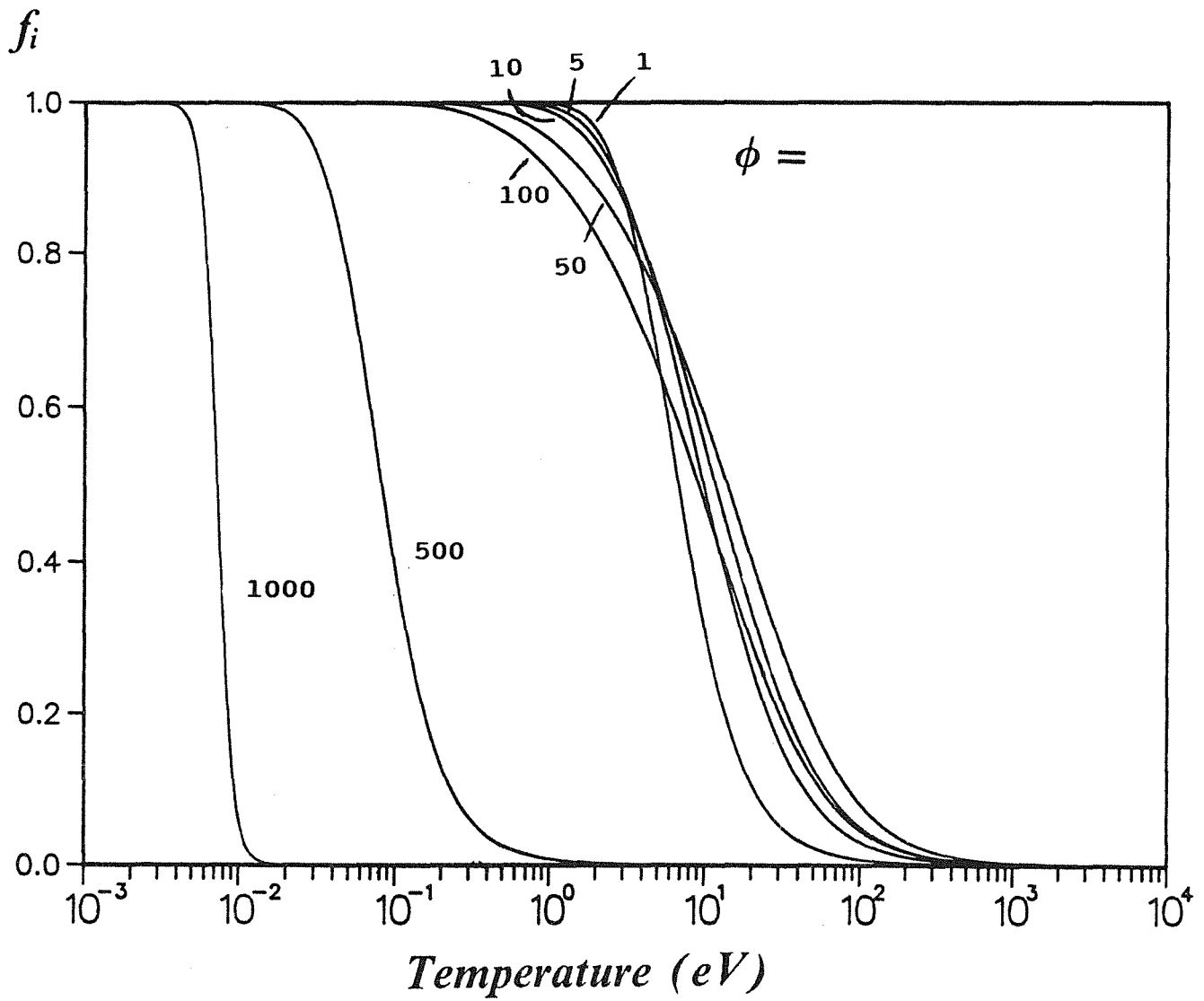


Figure 1A

The temperature and density dependent ionization fraction for hydrogen. Density is quoted with respect to LHD.

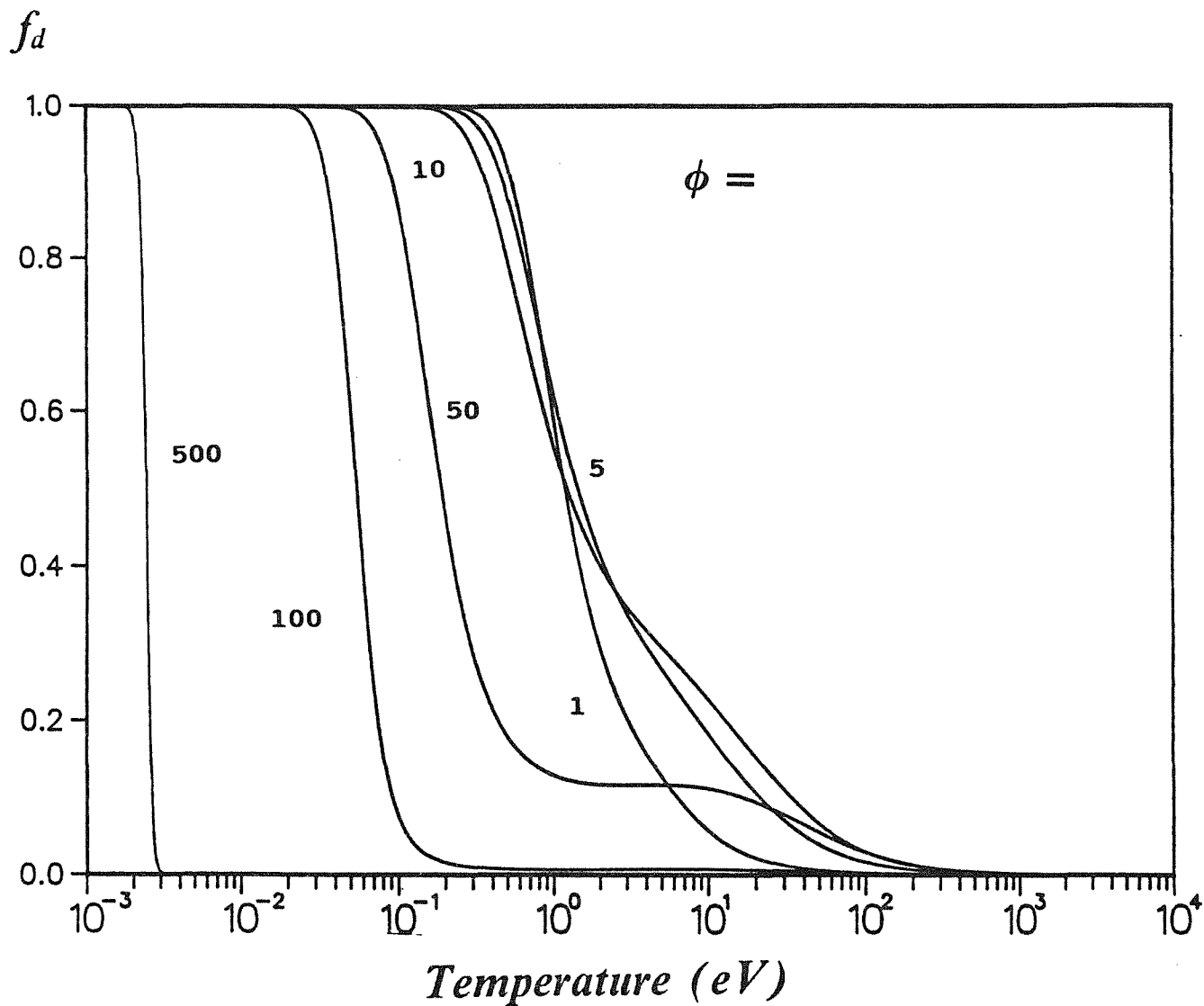


Figure 1B

The temperature and density dependent dissociation fraction for hydrogen. Density is quoted with respect to LHD.

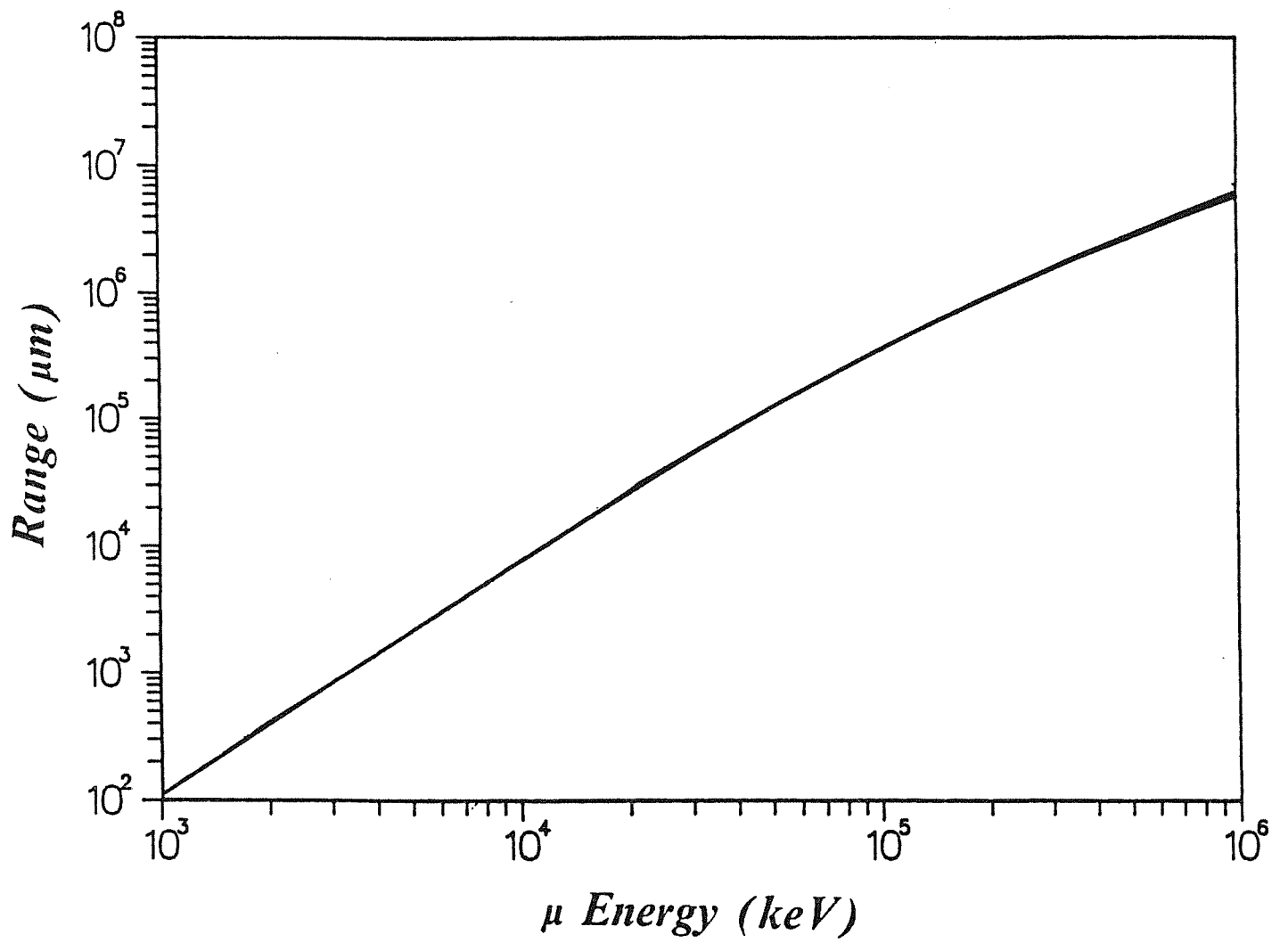


Figure 2

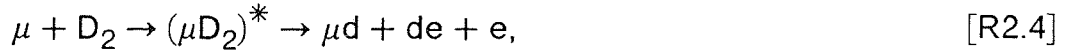
The average muon range in μm in 50%-50% deuterium-tritium fuel versus initial muon kinetic energy.

2.4 Muon capture

The formation of muo-hydrogen is little affected by the hydrogen isotope therefore the muo-deuterium and muo-tritium formation (muon capture) rates will be the same.

Note: Two different types of nomenclature will be used in representing reactions. This is necessary since some muon catalyzed fusion reactions include both chemical and nuclear interactions and in order to demonstrate the important facets of these reactions the normal chemical representations and the corresponding nuclear representations are intermixed. For example the bare deuterium or tritium nucleus can be represented by either D^+ and T^+ or d and t . As well the D_2 molecule can be written as $ddee$.

There are three ways in which muo-hydrogen may be formed (10). The first of these involves a muon and hydrogen molecule (D_2 or T_2) and therefore occurs at temperatures and densities prior to molecular dissociation. As a muon slows in hydrogen, the muon will be trapped by a hydrogen molecule and subsequent de-excitation of this complex molecule yields muo-atoms. The molecular capture reactions are:



and both have a reaction rate of

$$\lambda(\text{cap}) \sim 1.0 \times 10^{10} f_d \phi \quad (\text{s}^{-1}). \quad [E2.10]$$

Two further processes may occur when the medium is ionized which will form μt and μd . The first of these is radiative capture of a muon by a hydrogen ion (d or t).

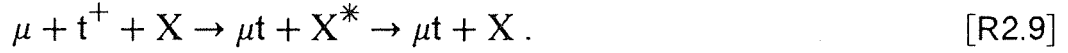


The reaction rate for the radiative capture reaction is

$$\lambda(\text{rc}) \sim 2.0 \times 10^6 T_{\text{eV}}^{-1/2} (1 - f_i) \phi \quad (\text{s}^{-1}). \quad [E2.11]$$

Capture of muon by a hydrogen ion may also occur by a three body reaction where electron interaction allows a radiationless transition between the muon and d or t . These reactions are rare at normal densities but, due to the non-linear density dependence, become important as density increases. The radiationless capture reactions are:





where X represents the third body i.e. an electron. The reaction rate for both radiationless capture reactions is

$$\lambda(\text{nrtb}) \sim 10^{18} T_{\text{eV}}^{-9/2} (1 - f_i)^2 \phi^2 \quad (\text{s}^{-1}). \quad [E2.12]$$

An important question to answer now is at what temperatures and densities do muo-atoms ionize. The energy required to excite any energy level in a muonic atom will be about the mass ratio of muon and electron times the electronic system energy. The muon is about 207 times the mass of an electron, therefore the ionization of μd or μt is 2663 eV and 2711 eV (14) respectively. If the temperature of the medium exceeds about 2.7 keV then muon catalyzed fusion will cease. Pressure ionization will not be a factor since densities (with respect to LHD) exceeding 10^9 (!) are required. A Saha equation for muo-atom ionization can be formulated, however it is simpler and sufficient to account for ionization by applying the following multiplier to any reaction rate that involves muo-atoms.

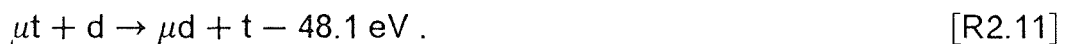
$$\left(1 - e^{-\frac{2700}{T_{\text{eV}}}}\right) \quad [E2.13]$$

The formation of μd and μt is assumed to occur at the same rate and is called λ_a . The temperature and density dependent muo-atom formation rates are summed from all mechanisms are plotted in Figure 3.

Figure 3 shows that muo-atom formation is large at temperatures less than 10 eV. The sharp jump at very low temperature and densities of 500-1000 demonstrate the effect of pressure ionization and a switch of the dominance from one formation mechanism to another. As the temperature increases above 10 eV the formation rate steadily decreases for all densities.

2.5 Muon transfer

Since μt has a 48.1 eV lower binding energy than μd the transfer of a muon from μd to a triton of some form (T_2 , t_e or t) is favourable (10). The reverse reaction, a muon transferring from μt to a deuteron is possible when the medium temperature exceeds 48.1 eV (this assumes that all transitions end in the $n=1$ energy level which is a gross simplification). The transfer reactions are:



The reaction rate for Reaction 2.10 is assumed to be the same for all temperatures and also assumed to have only a linear dependence with density.

$$\lambda_{dt} \sim 10^{10} \phi \quad (\text{s}^{-1}). \quad [E2.14]$$

The reaction rate for Reaction 2.11 will also be assumed constant with temperature for temperatures greater than 48.1 eV. An exponential rise in the reaction rate for Reaction 2.11 is assumed on approaching the critical temperature of 48.1 eV.

$$\lambda_{td} \sim 10^{10} e^{-\frac{48.1}{T_{\text{eV}}}} \phi \quad (\text{s}^{-1}). \quad [\text{E2.15}]$$

Figure 4 plots both λ_{dt} and λ_{td} from Equations 2.14 and 2.15 versus temperature for various fuel densities.

2.6 Muo-molecule formation

Mechanisms for muo-molecule formation, the precursors to muon catalyzed fusion, will be discussed here. As was mentioned earlier the function of the muon is to create a muo-molecular ion in which two hydrogen nuclei are confined. Direct interaction between a muo-atom and a normal atom, similar to standard no-muon fusion, still has a considerable Coulomb barrier to overcome. The formation rate for the direct process is calculated to be (15)

$$\lambda_{\mu dt}(\text{dir}) \sim 4 \times 10^3 \quad (\text{s}^{-1})$$

at LHD. The muo-molecular ion formation will always dominate this more direct fusion process.

In the description of the muo-molecular formation reaction mechanisms two important factors are not considered. When a muo-atom is formed, it may be in one of the two possible spin states. The spin states of muo-deuterium are $\mu d_{\frac{3}{2}}$ and $\mu d_{\frac{1}{2}}$ and the spin states of muo-tritium are μt_1 and μt_0 . The populations of the spin states are affected by the muo-atom formation mechanism and the collisional history of the muo-atom. The muo-atom's spin state will have an effect upon the muo-molecular formation. However, this effect is ignored since no clear method of calculating the spin state population as well as their effect upon the muo-molecular formation exists. Also, once muo-molecules are formed it is possible that they can break apart before they undergo fusion. This breakup rate must be known in order to calculate the effective formation rate. At high temperature and density an adequate theory does not exist to calculate the breakup rates. Their absence will tend to over-estimate the muo-molecular formation rate.

The temperature and density dependent muo-molecular formation rates are described via various possible mechanisms. With 50-50 deuterium-tritium fuel it is required to consider the formation mechanisms of μdd , μdt and μtt .

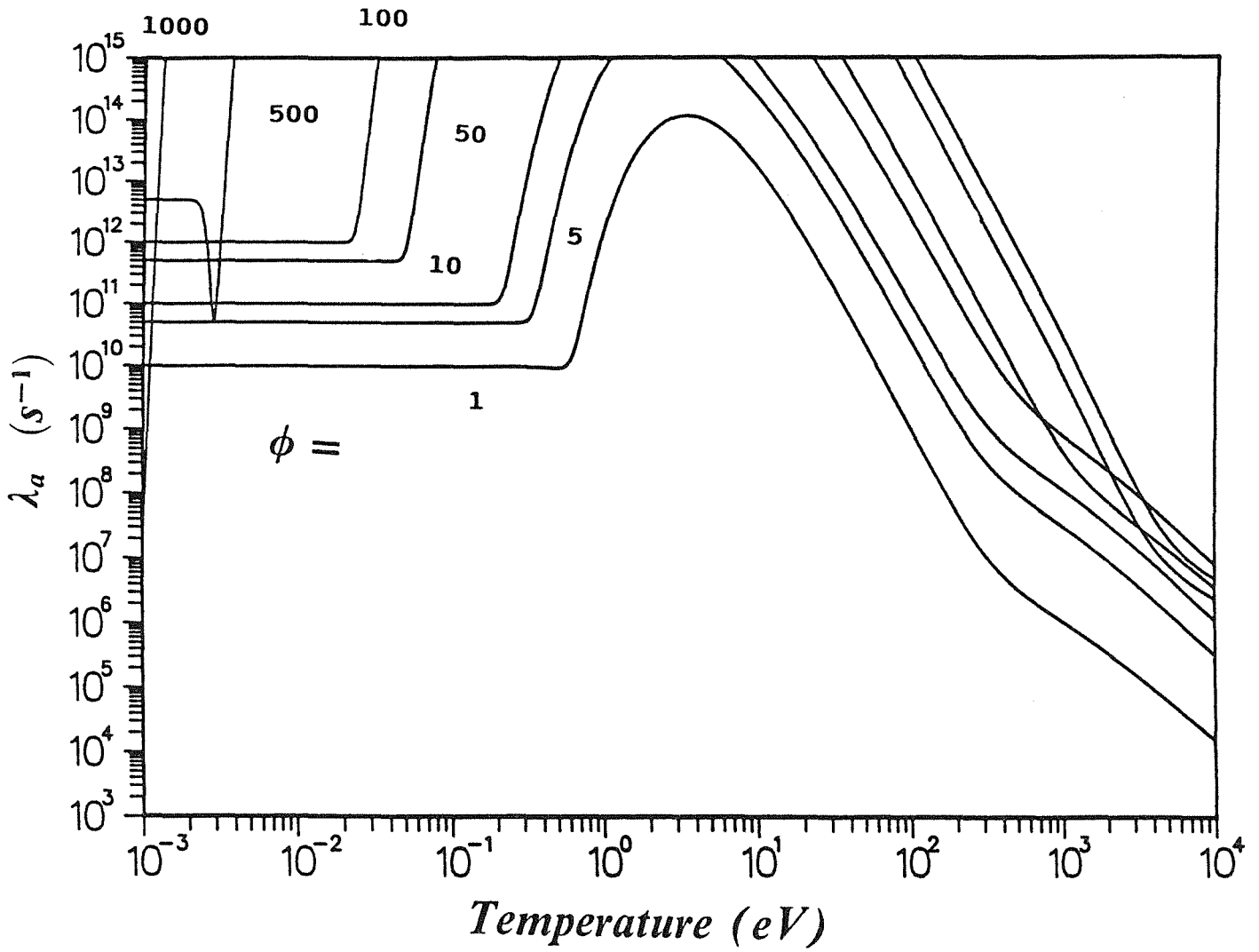


Figure 3

The temperature and density dependent muo-atom formation rate of deuterium or tritium.

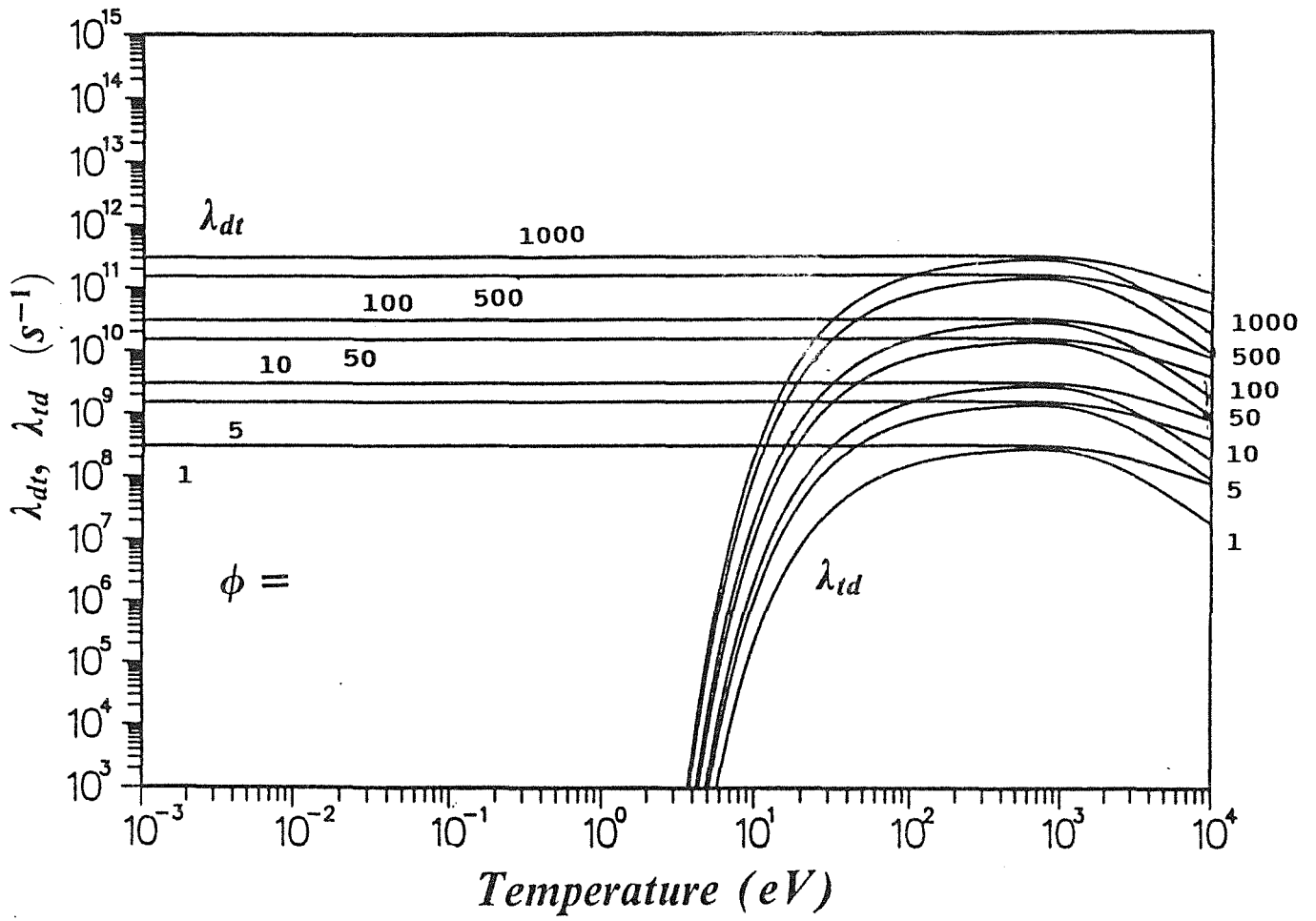


Figure 4

The temperature and density dependent muon transfer reaction rates. λ_{dt} represents muon transfer from deuterium to tritium and λ_{td} represents muon transfer from tritium to deuterium.

2.6.1 Resonant formation

A muo-molecule will be formed when a muo-atom combines with a fuel molecule, either D_2 or T_2 . Resonant formation of a muo-molecule may proceed if the difference between the binding energy of the muo-atom and the corresponding muo-molecule is low enough that it can be taken up by vibrational or rotational modes of the muo-molecule. If the difference is less than the dissociation energy of the hydrogen molecule (around 4.5 eV) then resonance formation can proceed. It turns out that there are only two possibilities: formation of μdd and formation μdt from μt and these occur preferably for muo-molecule rotational quantum number $J = 1$, and vibrational quantum number $v = 1$ (14). For the μdt reaction,



the binding energy difference between the muo-atom and the muo-molecule is

$$\varepsilon(11) = -0.7 \text{ eV} .$$

The reaction rate is

$$\lambda_{\mu dt}(\text{res}) \sim 10^7 T_{\text{eV}}^{-3/2} e^{\frac{-0.07}{T_{\text{eV}}}} C_d f_d \phi \quad (\text{s}^{-1}) \quad [\text{E2.16}]$$

where C_d represents the deuterium fraction of the fuel.

Similarly for the μdd reaction,



the binding energy difference is

$$\varepsilon = -2.0 \text{ eV} .$$

The reaction rate is

$$\lambda_{\mu dd}(\text{res}) \sim 4 \times 10^4 T_{\text{eV}}^{-3/2} e^{\frac{-0.0795}{T_{\text{eV}}}} C_d f_d \phi \quad (\text{s}^{-1}) . \quad [\text{E2.17}]$$

2.6.2 Non-resonant formation (electron emission)

If the excess energy formed from the formation of the muo-molecule is allowed to be taken away by an electron then by this non-resonant way μdd , μdt , and μtt formation are possible (10).

The non-resonant μdd formation reaction is



with a reaction rate of

$$\lambda_{\mu dd}(\text{nres}) \sim 5.0 \times 10^5 C_d f_d \phi \quad (\text{s}^{-1}). \quad [E2.18]$$

Since all the excess energy is taken by the electron, μdt may be formed by interaction of μt and D_2 or by interaction between μd and T_2 .

The non-resonant of μdt formation reactions are:



The reaction rates are respectively:

$$\lambda_{\mu td}(\text{nres}) \sim 5.0 \times 10^5 C_d f_d \phi \quad (\text{s}^{-1}) \quad [E2.19]$$

and

$$\lambda_{\mu dt}(\text{nres}) \sim 5.0 \times 10^5 C_t f_d \phi \quad (\text{s}^{-1}) \quad [E2.20]$$

where C_t represents the tritium fraction of the fuel.

Note: When a μt interacts to form a μdt muo-molecular the subscripts on reaction rates use μtd (t first) and when it is μd interacting the subscripts use μdt .

The non-resonant μtt formation reaction is



with a reaction rate of

$$\lambda_{\mu tt}(\text{nres}) \sim 5.0 \times 10^5 C_t f_d \phi \quad (\text{s}^{-1}). \quad [E2.21]$$

2.6.3 Direct Radiative Ion Capture

If the material is completely ionized it is possible that the muo-molecular ion can form directly with the emission of excess energy in the form of a gamma ray (10).

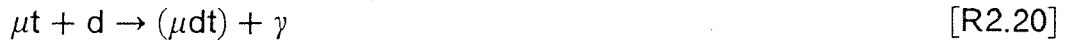
The direct radiative ion capture formation of μdd reaction is



with a reaction rate of

$$\lambda_{\mu dd}(dr) \sim 1.8 \times 10^5 T_{eV}^{-1/2} (1 - f_i) C_d \phi \quad (s^{-1}). \quad [E2.22]$$

The direct radiative ion capture formation of μdt reactions are



with reaction rates respectively

$$\lambda_{\mu dt}(dr) \sim 1.8 \times 10^5 T_{eV}^{-1/2} (1 - f_i) C_t \phi \quad (s^{-1}) \quad [E2.23]$$

and

$$\lambda_{\mu td}(dr) \sim 1.8 \times 10^5 T_{eV}^{-1/2} (1 - f_i) C_d \phi \quad (s^{-1}). \quad [E2.24]$$

Similarly, the direct radiative ion capture formation of the μtt reaction is



with a reaction rate of

$$\lambda_{\mu tt}(dr) \sim 1.8 \times 10^5 T_{eV}^{-1/2} (1 - f_i) C_t \phi \quad (s^{-1}). \quad [E2.25]$$

2.6.4 Dissociative formation

Lane (16) suggests a two body reaction between a muo-atom and a molecule, where the excess energy created by muo-molecule formation is used to dissociate the molecule. This process takes place only for the following two reactions:



which has a reaction rate of

$$\lambda_{\mu dt}(\text{Lane}) \sim 5 \times 10^{11} T_{eV}^{1/2} e^{-\frac{4.0}{T_{eV}}} f_d C_d \phi \quad (s^{-1}) \quad [E2.26]$$

and



which has a reaction rate of

$$\lambda_{\mu dd}(\text{Lane}) \sim 5 \times 10^{11} T_{eV}^{1/2} e^{-\frac{2.7}{T_{eV}}} f_d C_d \phi \quad (s^{-1}). \quad [E2.27]$$

2.6.5 Three body reactions

Men'shikov and Ponamarev (17) formulated three body mechanisms for formation of μdt in atomic or ionized hydrogen. The possible three body reactions are



Here X represents another hydrogen (d or t) atom or an electron. The reaction rate of Reactions 2.24 and 2.25 combined is

$$\lambda_{\mu dt}(\text{MPf}) \sim 6.0 \times 10^{10} T_{eV}^{-3/2} (1 - f_i) f_i C_d \phi^2 \quad (s^{-1}). \quad [E2.28]$$

For each of the possible muo-molecules, the muo-molecular formation rates are calculated by summing all possible formation mechanisms and are plotted in Figures 5 - 8.

The temperature and density dependent μdd formation rate is plotted in Figure 5. Since pressure ionization begins to play a major role at fuel densities between 100 and 1000 (with respect to LHD), a change in the formation mechanisms in this density range is expected. This is clearly demonstrated in Figure 5 where the temperature dependent μdd formation rate for densities 500 and 1000 depends primarily upon ion capture mechanisms and at lower densities molecular processes (i.e. resonant and non-resonant molecular capture) dominate. The magnitude of the μdd formation rate at temperatures less than 0.2 eV is low (but linearly dependent on density). At temperatures greater than 0.2 eV and for densities of 100 and less, the formation rate becomes large due to the molecular dissociative formation process (Lane mechanism).

The temperature and density dependent μdt formation occurs via two routes. Formation of μdt with μd atom is plotted in Figure 6. The reaction rates are low at low temperatures and as temperature increases they steadily decrease for all densities. Formation of μdt via μt is plotted in Figure 7. For densities of 50 and less and temperatures less than 1 eV the μdt formation rate is dominated by the resonant formation. At higher temperatures three body reactions and dissociative formation mechanisms dominate. Due to the density dependence of these mechanisms and especially the density and temperature dependence of the dissociation and ionization fractions of deuterium and tritium molecules (see Figures 1A and 1B), the μdt formation rate tends to maximize between 1 eV and 10 eV as the density increases. At large densities (greater than 100) the fuel is completely ionized and high temperature formation becomes small.

The density and temperature dependent μtt formation rate is plotted in Figure 8. The curves are the same as those in Figure 6 due to the same formation mechanisms at work.

2.7 Nuclear fusion

The pair of hydrogen isotopes in a muo-molecular ion will be very close together and the probability of tunneling through the reduced Coulomb barrier is high. The fusion rates of μdd^+ , μdt^+ and μtt^+ are (10,18):

$$\lambda_{fdd} \sim 10^9 \text{ (s}^{-1}\text{)},$$

$$\lambda_{fdt} \sim 10^{12} \text{ (s}^{-1}\text{)},$$

$$\lambda_{ftt} \sim 10^7 \text{ (s}^{-1}\text{)}.$$

2.8 Muon sticking

After the fusion event has taken place, energy is released in the form of the kinetic energy of the reaction products and the muon will be released to catalyze further fusion reactions. The chain of reactions will end when a muon decays or the muon is lost from the system. The primary loss of muons, other than decay, will be when a muon is attached to a $Z > 1$ fusion byproduct (h or ^3He for μdd fusion and α or ^4He for μdt and μtt fusion). At the moment of fusion there is a certain probability of the muon being attached to the fusion byproduct. Once a muo-helium atom forms it is very difficult for the muon to be released and contribute to further fusions, however it is possible for the muon to be stripped away from the muo-helium and be regenerated. The regeneration probability will depend upon the density and temperature of the fuel and the initial energy of the muo-helium. In μdt fusion, the initial energy of the $\mu\alpha$ will be 3.5 MeV. At low fuel temperatures the primary stopping mechanism will be ionization of the fuel atoms and will generally yield regeneration probabilities around 20 % . The sticking probabilities (includes regeneration) for low temperatures and liquid hydrogen densities are (18):

$$w_{\text{dd}}(\text{initial}) \sim 0.12 ,$$

$$w_{\text{dt}}(\text{initial}) \sim 0.0045 ,$$

$$w_{\text{tt}}(\text{initial}) \sim 0.14 .$$

If the fuel is hot and semi-ionized the regeneration will increase. Since the normal energy loss of the energetic muo-helium decreases, there is a greater probability of muon stripping (19). It is difficult to model the sticking at high density and temperature, however in the current analysis calculations will be performed without sticking. If positive results exist for the no-sticking case then further analysis of sticking at high temperature and density is warranted, however if a negative result appears for the no-sticking case then any possible scheme is further doomed by sticking.

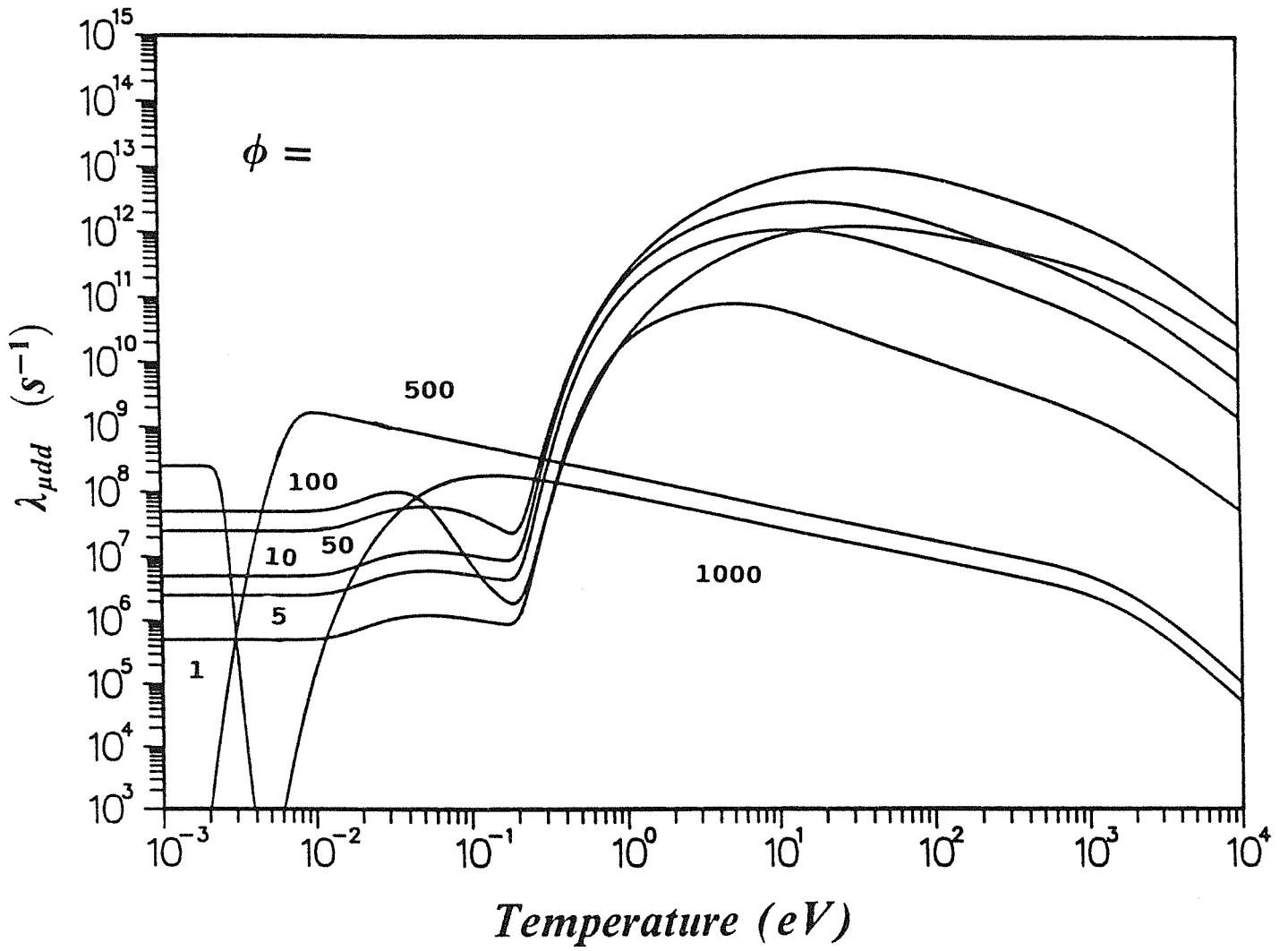


Figure 5

The temperature and density dependent μdd formation rate.

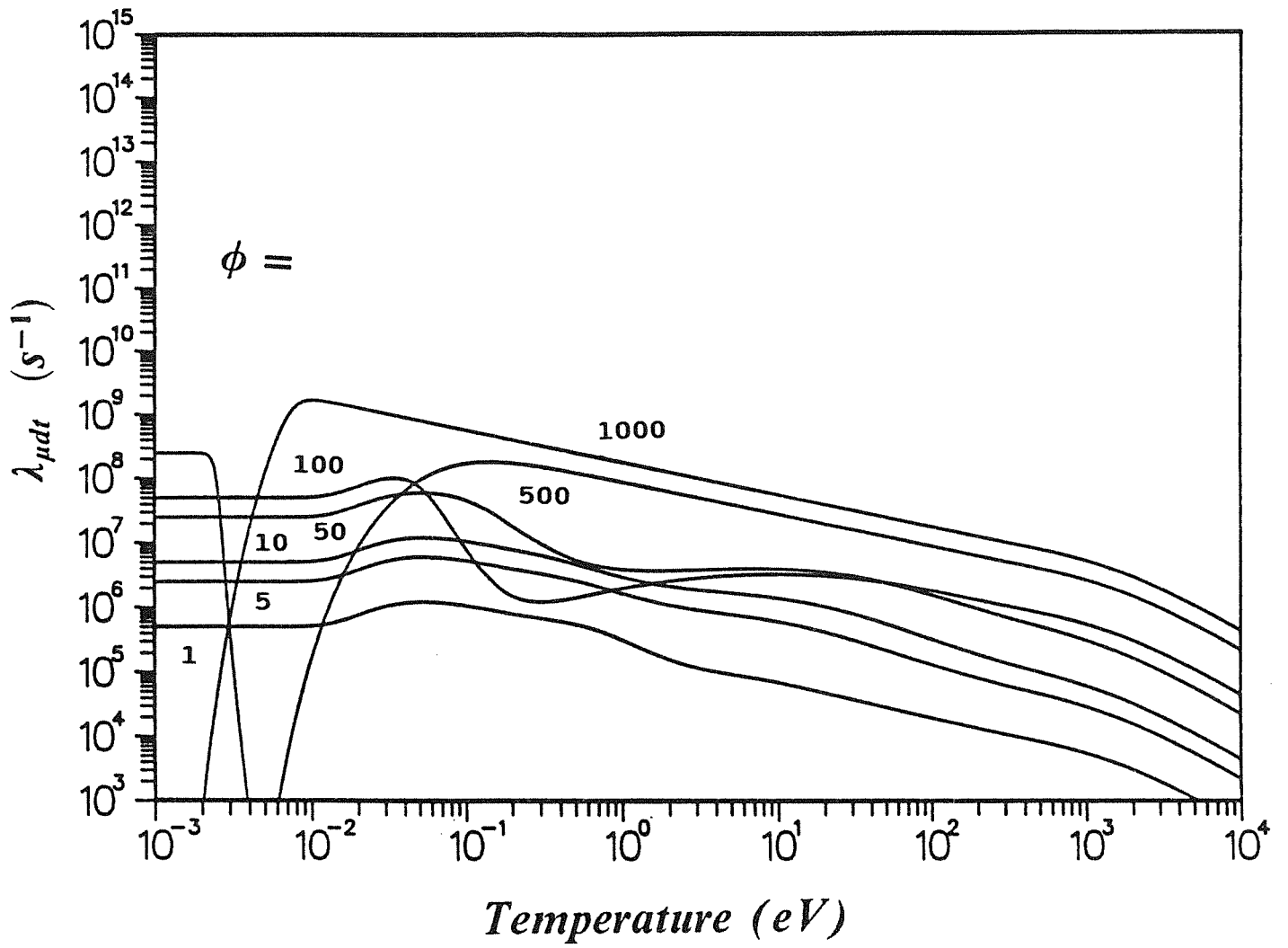


Figure 6

The temperature and density dependent μdt formation rate via muo-deuterium.

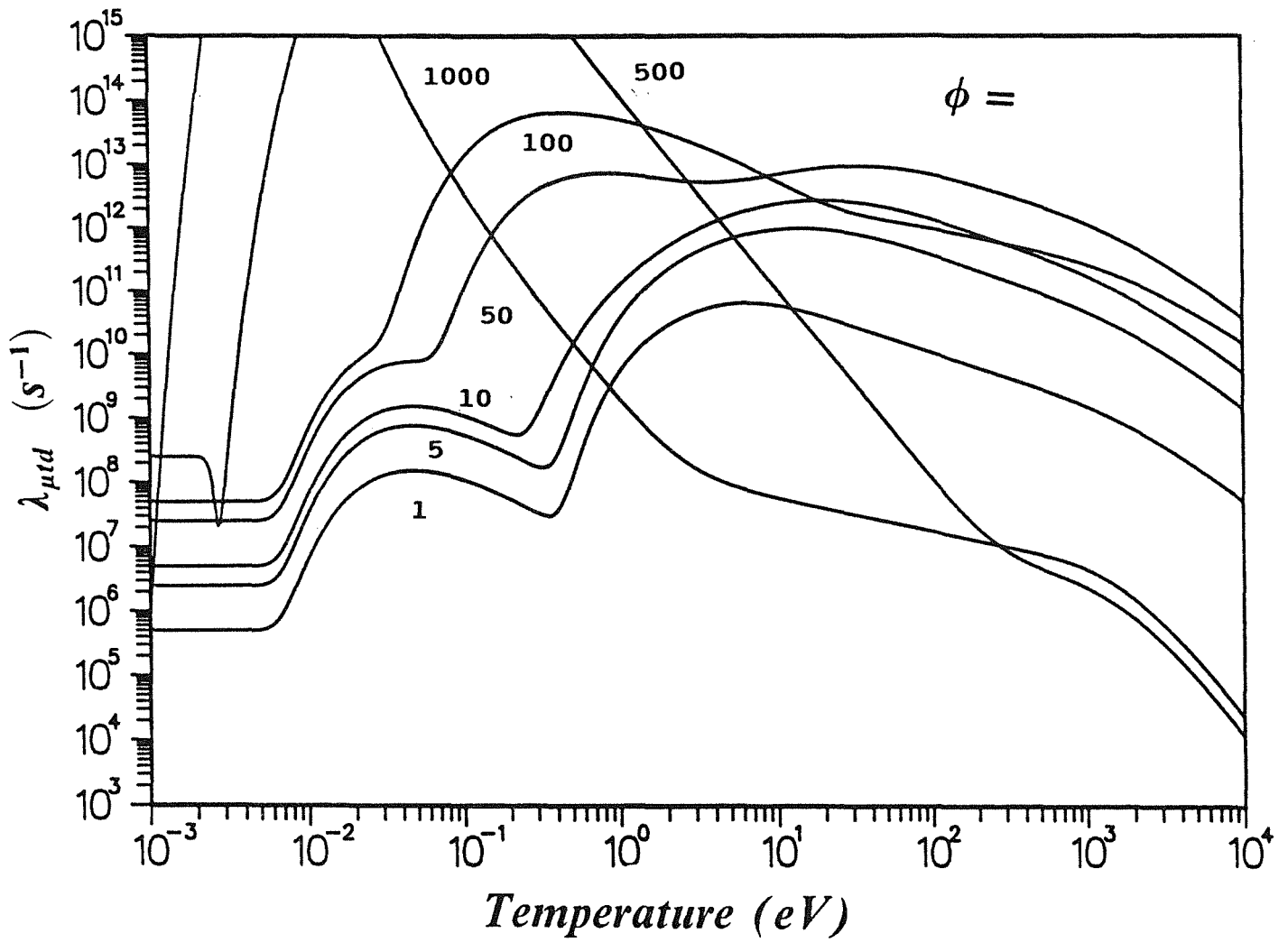


Figure 7

The temperature and density dependent μdt formation rate via muo-tritium.

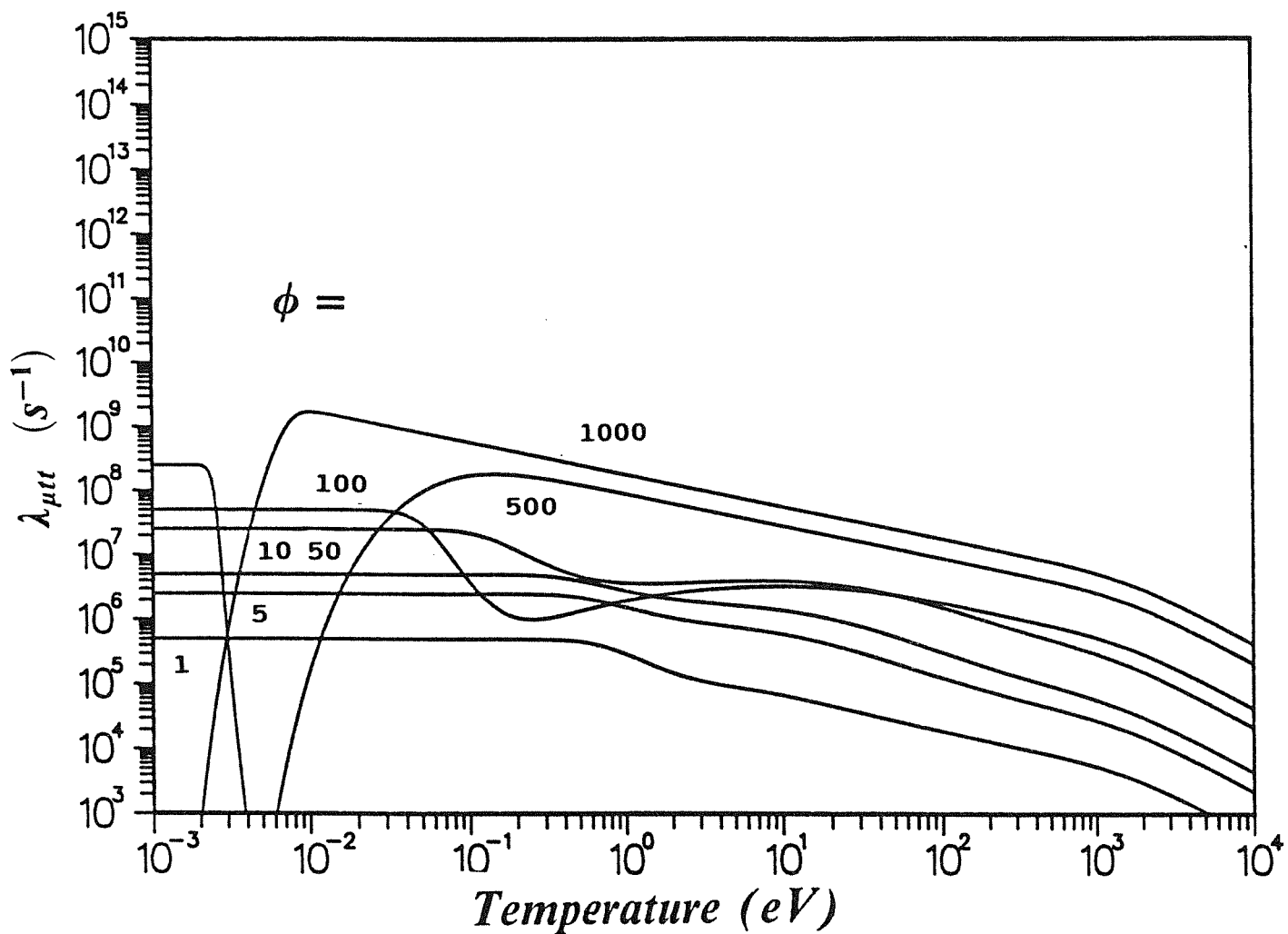


Figure 8

The temperature and density dependent $\mu\tau$ formation rate.

2.9 Kinetics

Using the previously defined muon catalyzed fusion reaction rates it is possible to write a set of kinetic equations describing the concentrations of muons, muo-atoms and muo-molecules (20,21). The full set of reactions are displayed in Figure 9. This reaction set differs from standard schemes in that it includes the formation of μdt and the muon transfer from μd . The concentrations of μ , μd , μt , μdd , μdt , μtt , are represented in the following reaction set by: N_μ , $N_{\mu d}$, $N_{\mu t}$, $N_{\mu dd}$, $N_{\mu dt}$, $N_{\mu tt}$.

$$\frac{dN_\mu}{dt} = -\lambda_a N_\mu + \lambda_{fdd} (1 - f(1 - w_{dd})) N_{\mu dd} + \lambda_{fdt} (1 - w_{dt}) N_{\mu dt} + \lambda_{ftt} (1 - w_{tt}) N_{\mu tt} \quad [E2.29]$$

$$\frac{dN_{\mu d}}{dt} = \lambda_a C_d N_\mu - (\lambda_{dt} C_t + \lambda_{\mu dt} C_t + \lambda_{\mu dd} C_d + \lambda_\mu) N_{\mu d} + \lambda_{td} C_d N_{\mu t} \quad [E2.30]$$

$$\frac{dN_{\mu t}}{dt} = \lambda_a C_t N_\mu + \lambda_{dt} C_t N_{\mu d} - (\lambda_{td} C_d + \lambda_{\mu td} C_d + \lambda_{\mu tt} C_t + \lambda_\mu) N_{\mu t} \quad [E2.31]$$

$$\frac{dN_{\mu dd}}{dt} = \lambda_{\mu dd} C_d N_{\mu d} - (\lambda_{fdd} + \lambda_\mu) N_{\mu dd} \quad [E2.32]$$

$$\frac{dN_{\mu dt}}{dt} = \lambda_{\mu dt} C_t N_{\mu d} + \lambda_{\mu td} C_d N_{\mu t} - (\lambda_{fdt} + \lambda_\mu) N_{\mu dt} \quad [E2.33]$$

$$\frac{dN_{\mu tt}}{dt} = \lambda_{\mu tt} C_t N_{\mu t} - (\lambda_{ftt} + \lambda_\mu) N_{\mu tt} \quad [E2.34]$$

The value of f is found experimentally to be about 0.43 (22).

The rate of fusion reactions are calculated with the following equations:

$$\frac{dN_{fdd}}{dt} = \lambda_{fdd} N_{\mu dd}, \quad [E2.35]$$

$$\frac{dN_{fdt}}{dt} = \lambda_{fdt} N_{\mu dt}, \quad [E2.36]$$

$$\frac{dN_{ftt}}{dt} = \lambda_{ftt} N_{\mu tt}. \quad [E2.37]$$

It is possible to reduce the above set of reactions to an extent that only two parameters for each muo-molecule are needed to describe it. Figure 9 shows a muon 'cycling' though various reactions eventually leading to fusion muon decay or muon loss by sticking to helium. After fusion the released muons will begin the reaction chain again. This reaction network can be simplified to the reaction scheme illustrated in Figure 10. An equation set can be formulated to describe this simplified scheme and is as follows:

$$\frac{dN_{\mu}}{dt} = -(\lambda_{\mu} + \lambda_c w_s) N_{\mu}, \quad [E2.38]$$

$$\frac{dN_f}{dt} = \lambda_c N_{\mu} \quad [E2.39]$$

where

N_{μ} is the number of muons injected ,

N_f is the total number of fusion reactions ,

λ_{μ} is the average muon decay rate ,

λ_c is the effective muon cycling rate and

w_s is the effective sticking probability .

For each of the possible muo-molecules: μdd , μdt , μtt there will be a corresponding λ_c and w_s .

Gershtein et.al. (20) developed a method of taking the full dynamic and reducing it to a cycling rate and effective sticking probability (in principle this is straight forward since all equations are linear, however with more than 2 equations the calculations become exponentially more tedious). Gershtein's paper did not consider muon transfer from μt to d and the formation of μdt from μd and t . Also this paper greatly simplified the analysis by assuming that the rates of formation of muo-atoms are very much greater than other formation processes, however this may not be true at high temperatures (see Figure 3). As well the fusion rates of μdd , μdt and μtt were assumed to be very much faster than any other process. The fusion rate for μdt is indeed faster than most processes considered in this report, however the fusion rate of μdd and μtt will be the rate determining step for some temperatures and densities of interest here. In order to combine the dynamics of the muo-molecular formation rates and the fusion rates and not to excessively complicate the analysis, the cycling rate will be calculated as a parallel combination of the muo-atom formation rate, the fusion rate and the cycling rate that is calculated when the muo-atom formation rate and fusion rate are assumed to be very large.

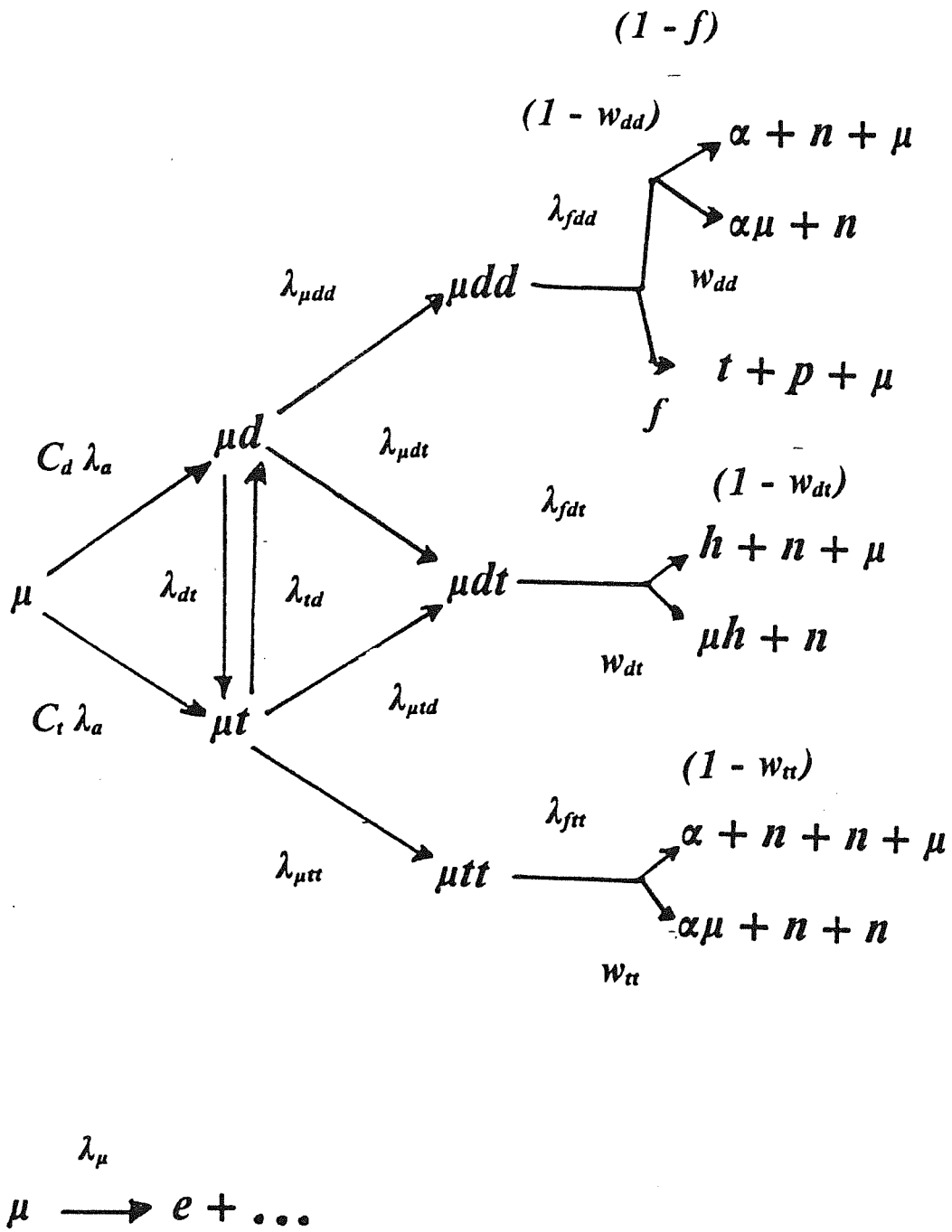


Figure 9

The muon catalyzed fusion reaction network in deuterium-tritium fuel.

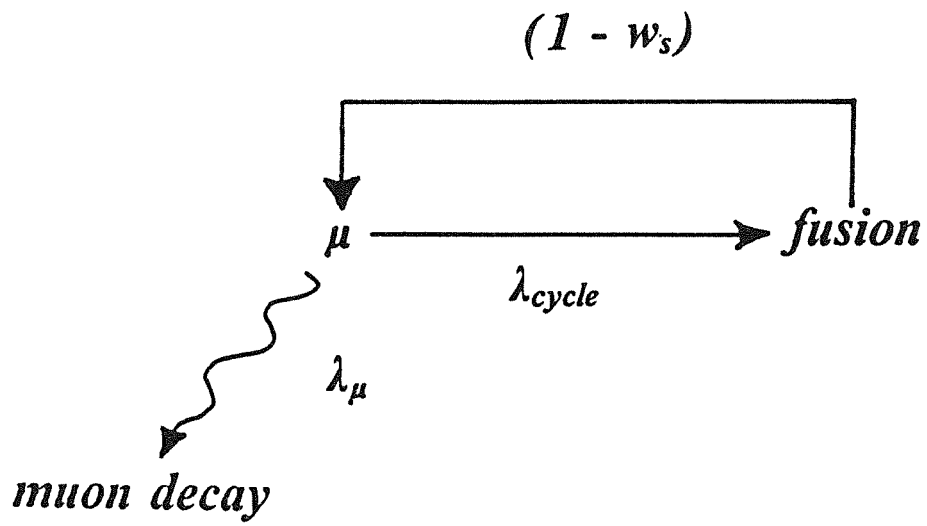


Figure 10

The simplified muon catalyzed fusion reaction network.

Using the method of Gershtein et. al. and the points above, the cycling rate for μdd formation is calculated with

$$\frac{1}{\lambda_c(\mu dd)} = \frac{\lambda_\mu + \alpha_1 + \alpha_2}{C_d \lambda_{\mu dd} (C_d \lambda_\mu + \alpha_2)} + \frac{1}{\lambda_a} + \frac{1}{\lambda_{fdd}}, \quad [E2.40]$$

for μdt formation the muon cycling rate is calculated with

$$\frac{1}{\lambda_c(\mu dt)} = \frac{\lambda_\mu + \alpha_1 + \alpha_2}{C_t \lambda_{\mu dt} (C_d \lambda_\mu + \alpha_2) + C_d \lambda_{\mu dt} (C_t \lambda_\mu + \alpha_1)} + \frac{1}{\lambda_a} + \frac{1}{\lambda_{fdt}}. \quad [E2.41]$$

and for μtt formation with

$$\frac{1}{\lambda_c(\mu tt)} = \frac{\lambda_\mu + \alpha_1 + \alpha_2}{C_t \lambda_{\mu tt} (C_t \lambda_\mu + \alpha_1)} + \frac{1}{\lambda_a} + \frac{1}{\lambda_{ftt}}, \quad [E2.42]$$

where:

$$\alpha_1 = C_t \lambda_{dt} + C_t^2 \lambda_{\mu dt} + C_d C_t \lambda_{\mu dd},$$

$$\alpha_2 = C_d \lambda_{td} + C_d^2 \lambda_{\mu td} + C_d C_t \lambda_{\mu tt}.$$

Using Equations 2.40, 2.41 and 2.42, the temperature and density dependant cycling rate of μdd , μdt and μtt are plotted in Figures 11, 12 and 13 respectively. The total muon cycling rate is calculated by summing the muon cycling rates of μdd , μdt and μtt and is plotted in Figure 14.

$$\lambda_c(\text{total}) = \lambda_c(\mu dd) + \lambda_c(\mu dt) + \lambda_c(\mu tt). \quad [E2.43]$$

The muon cycling rates of μdd (Figure 11) and μtt (Figure 13) are limited by their respective fusion rates. Comparing the μdt muon cycling rate (Figure 12) to the total muon cycling rate (Figure 14) it is evident that μdt rate dominates. Comparing the μdt muon cycling rate (Figure 12) to the μdt formation rate (Figure 7) it is clear that the μdt formation dominates the muon catalyzed fusion reaction dynamics in 50-50 deuterium-tritium fuel.

The total sticking probability is

$$w_s(\text{total}) = \frac{\lambda_c(\mu dd) w_s(\mu dd) + \lambda_c(\mu dt) w_s(\mu dt) + \lambda_c(\mu tt) w_s(\mu tt)}{\lambda_c(\text{total})}. \quad [E2.44]$$

Even though the μdd and μtt muon cycling rates are small compared to μdt the fact that the muon sticking co-efficients associated with μdd and μtt fusion are much larger than with μdt fusion means these muon cycling rates are important.

Solving Equation 2.38 assuming relatively constant values of λ_c and w_s and an initial muon concentration of $N_\mu(0)$ yields,

$$N_\mu(t) = N_\mu(0) e^{-(\lambda_\mu + \lambda_c w_s)} \quad [E2.45]$$

where λ_μ is the average muon decay rate and is equal to $4.545 \times 10^5 \text{ s}^{-1}$.

The timing of compression and of muon catalyzed fusion reactions must be of similar magnitude for sufficient fusions to occur. In general the muon catalyzed fusion reactions occur over a mean muon lifetime ($1/\lambda_\mu \sim 2 \mu\text{s}$), however the number of muons and subsequently the fusion reaction rate will exponentially decrease as in Equation 2.45. If the cycling rate is high and/or the sticking is low the exponential decay is due only to muon decay. It is expected that compression times can be stretched to 100 - 200 ns and therefore the fusion reaction rate will remain rather flat for this time only if $\lambda_c w_s \ll \lambda_\mu$.

The average number of fusions per muon X_μ , can be calculated using equation 2.45 and integrating Equation 2.39 from time equals 0 to ∞ .

$$X_\mu(\infty) = \frac{\lambda_c}{\lambda_\mu + \lambda_c w_s} \quad [E2.46]$$

Since the compression time of the fuel is expected to be much less than the average muon lifetime, the effective number of fusions per muon can be approximated by

$$X_\mu(\text{eff}) \sim X_\mu(\infty) \frac{t_c}{2.2\mu\text{s}} \quad [E2.47]$$

where t_c is the compression time.

With the compression times approaching 200 ns, the effective number of fusions per muon for muon catalyzed fusion under compression will be at best an order of magnitude less than for the infinite reaction time case.

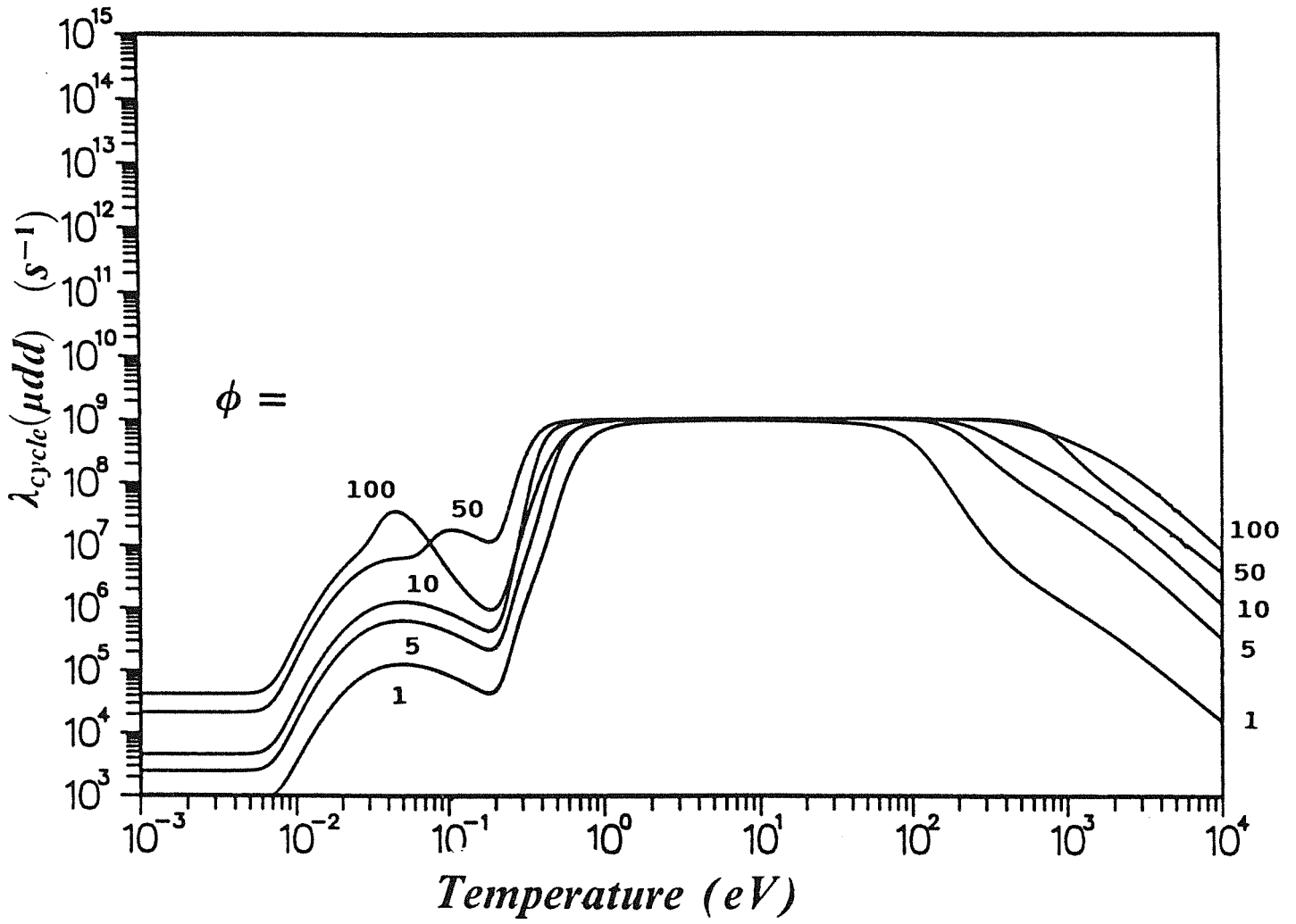


Figure 11

The temperature and density dependent muon cycling rate for the muon catalyzed fusion reaction via μdd .

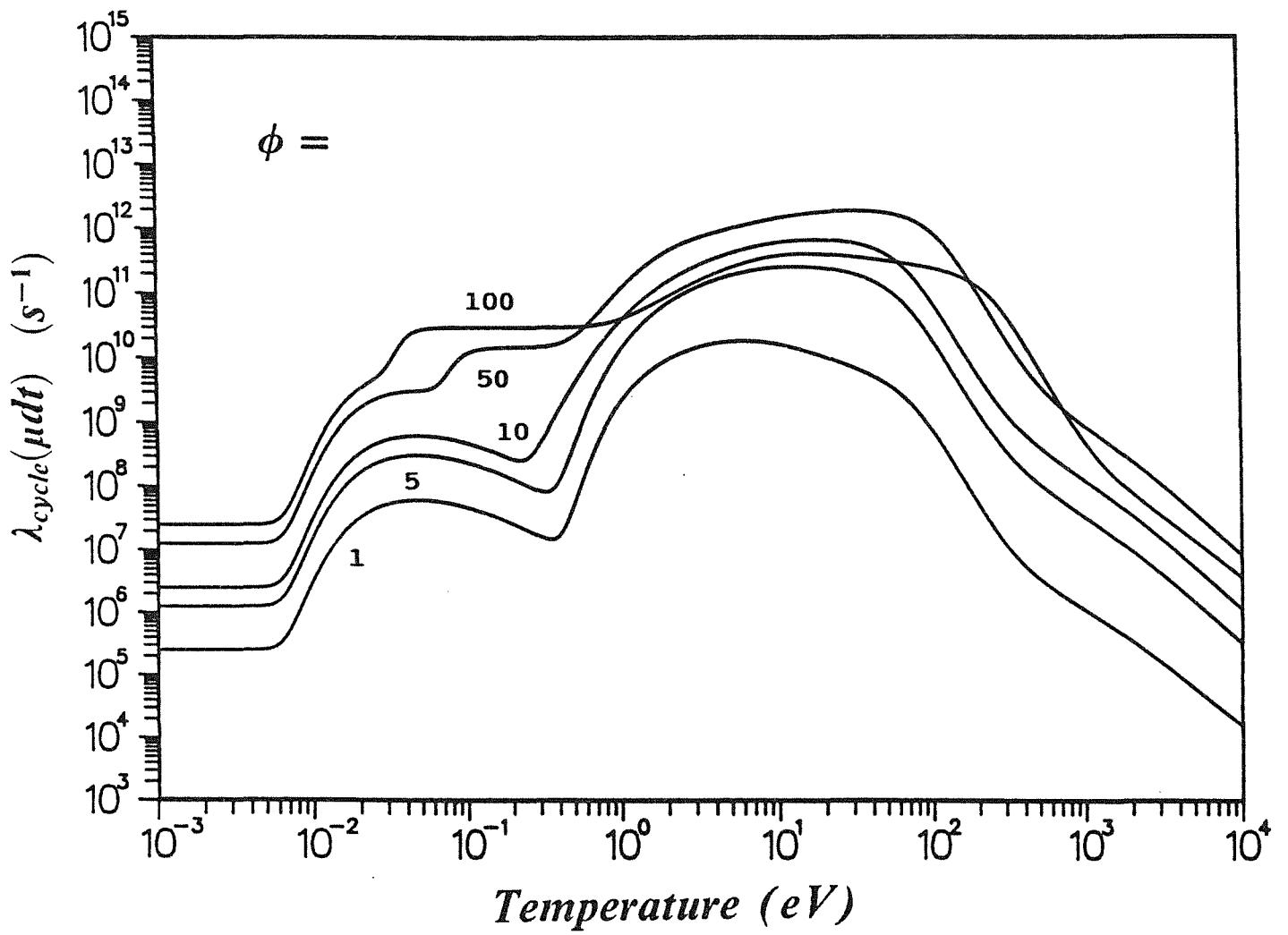


Figure 12

The temperature and density dependent muon cycling rate for the muon catalyzed fusion reaction via μdt .

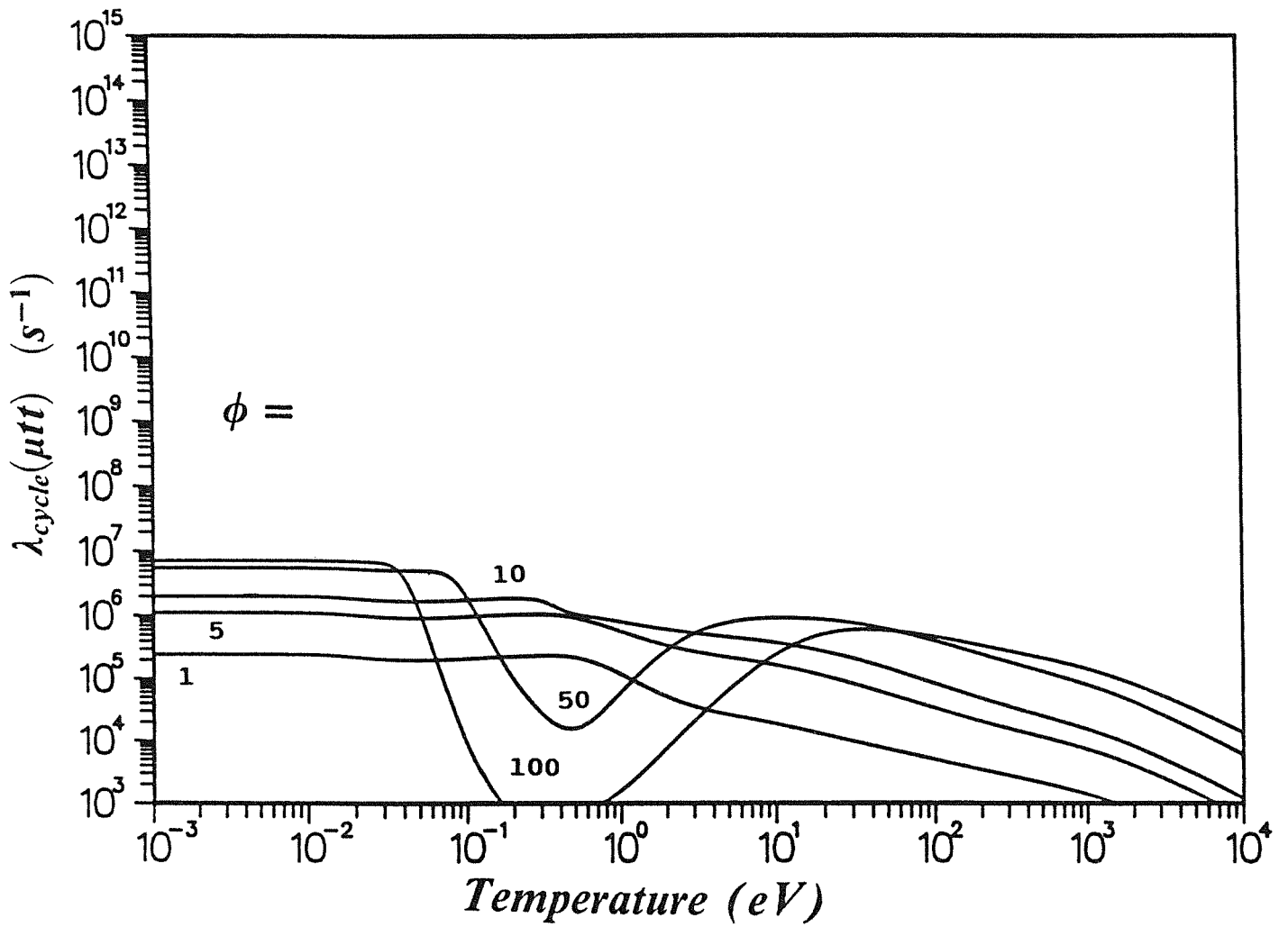


Figure 13

The temperature and density dependent muon cycling rate for the muon catalyzed fusion reaction via μtt .

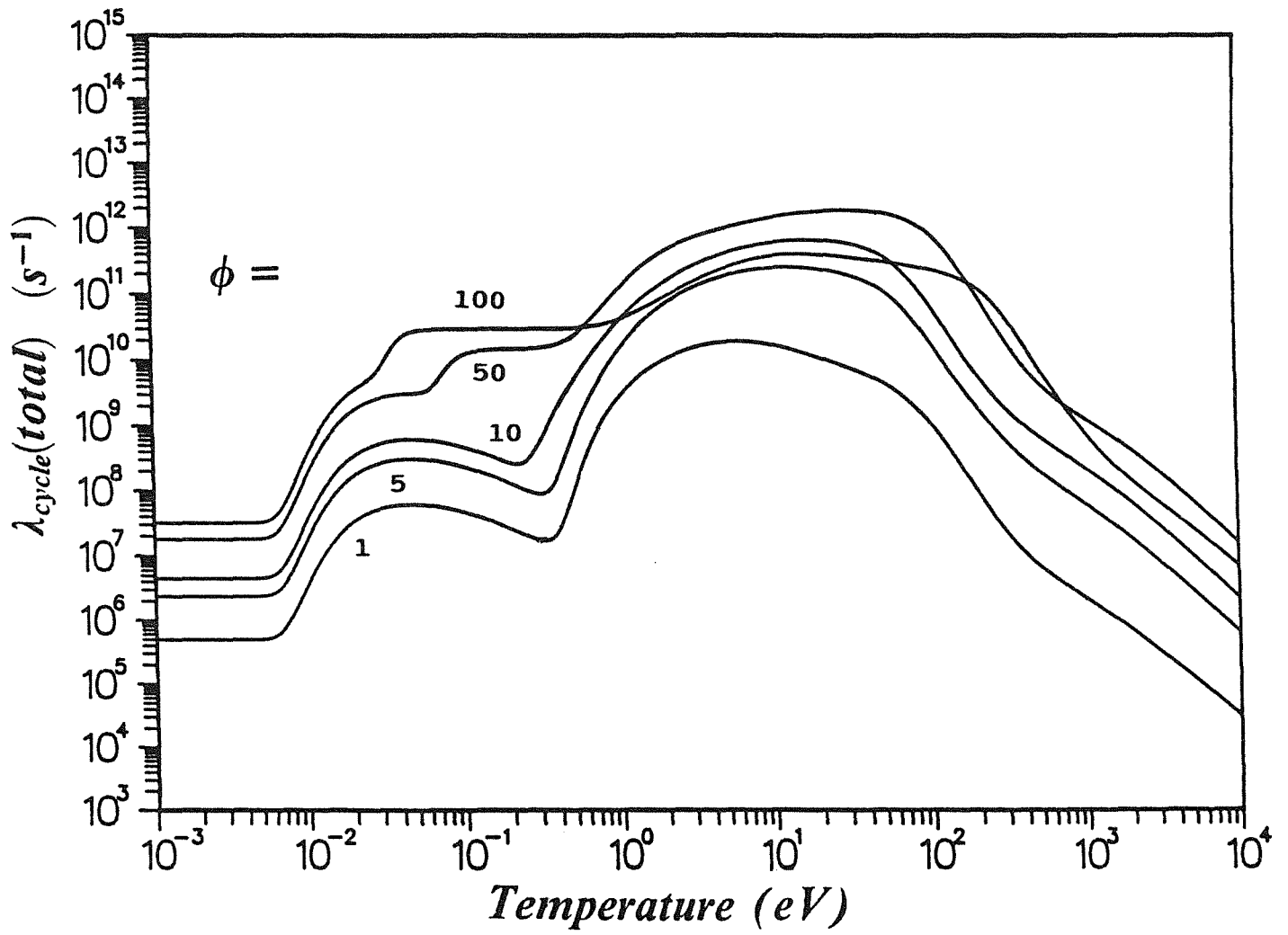


Figure 14

The total temperature and density dependent muon cycling rate.

3. Energy Balance Calculation

In this section the energy balance of a general muon catalyzed fusion system under compressive conditions is considered. Efficiencies of energy conversion, muon production and transfer, etc. are not included in order that a clear view of only the constraints of the muon catalyzed fusion reactions themselves is gained. The derived expressions are kept general, however only 50-50 deuterium-tritium fuel is specifically considered.

The energy gain is defined as

$$X = \frac{E_{out}}{E_{in}} \quad [E3.1]$$

3.1 E_{out}

The dominant muon catalyzed fusion and standard fusion reactions in a 50-50 deuterium-tritium fuel involve only deuterium-tritium fusion and therefore only these fusion reactions are considered. E_{out} has two potential sources, energy from muon catalyzed fusion $E_{\mu CF}$ and standard fusion reactions E_{SF} and therefore

$$E_{out} = E_{\mu CF} + E_{SF} \quad [E3.2]$$

The total energy generated from muon catalyzed fusion is

$$E_{\mu CF} = N_{\mu} E_f X_{\mu} \quad [E3.3]$$

where

N_{μ} is the number of muons injected ,

E_f is the energy released per fusion and

X_{μ} is the average number of fusions per muon .

The total energy generated from standard fusion is

$$E_{SF} = \frac{N_f}{2} E_f f_b \quad [E3.4]$$

where

N_f is the number of fuel atoms ,

E_f is the energy released per fusion and

f_b is the fuel burnup fraction .

Note: If the fuel starts to burn by standard fusion (ignited state) the value of f_b is assumed to be due to only standard fusion.

3.2 E_{in}

The energy investment is required to generate muons and to provide compression of the fuel. Muons will have an energy cost E_m and the compression energy is E_c thus

$$E_{in} = E_m + E_c \quad [E3.5]$$

The total energy cost of injected muons is

$$E_m = N_\mu E_\mu \quad [E3.6]$$

where

N_μ is the total number of muons injected and

E_μ is the energy cost of one muon .

The total energy required by an external driver to compress the fuel to a given density can be approximated by assuming that the fuel behaves as a fermi degenerate gas having an internal energy of (23)

$$E_{fdg} = 0.3 \phi^{\frac{2}{3}} r_o^3 \quad (\text{MJ}) \quad [E3.7]$$

where ϕ is the fuel density with respect to LHD and r_o is the initial radius of the fuel pellet (assumes spherical geometry).

During the reaction time of the fuel (the reaction time is the compression time), energetic fusion products will deposit their energy in the fuel. Prior to ignition in standard fusion this 'boot-strap' heating is not severe, however, muon catalyzed fusion reactions occur even at low temperatures. Fuel heating due to muon catalyzed fusion requires additional driver energy to achieve the desired density or just to offset the internal pressure and keep the fuel's integrity long enough for sufficient reactions to occur. Minimally, the extra energy required is

$$E_c(\mu CF) = N_\mu E_d X_\mu \quad [E3.8]$$

where E_d is the fusion energy deposited into the fuel.

The total energy required to compress the fuel is

$$E_c \sim E_c(\mu\text{CF}) + E_{fdg} = 0.3 \phi^{\frac{2}{3}} r_o^3 + N_\mu E_d X_\mu. \quad [\text{E3.9}]$$

Putting all these terms together yields an expression for the energy gain,

$$X = \frac{\frac{N_f}{2} E_f f_b + N_\mu E_f X_\mu}{0.3 \phi^{\frac{2}{3}} r_o^3 + N_\mu E_d X_\mu + N_\mu E_\mu}. \quad [\text{E3.10}]$$

Two cases can now be considered: first when muon catalyzed fusion dominates the energy gain and the other is when muon catalyzed fusion ignites standard type fusion.

3.3 Energy gain dominated by muon catalyzed fusion

Assuming that standard fusion burn-up f_b is minimal (this is a valid approximation if the fuel stays below 1 keV) then the energy balance is described by

$$X \sim \frac{N_\mu E_f X_\mu}{0.3 \phi^{\frac{2}{3}} r_o^3 + N_\mu (E_d X_\mu + E_\mu)}. \quad [\text{E3.11}]$$

In order to maximize X it is required that

$$N_\mu \gg \frac{0.3 \phi^{\frac{2}{3}} r_o^3}{(E_d X_\mu + E_\mu)}. \quad [\text{E3.12}]$$

If enough muons are used such that Equation 3.12 holds then the energy balance reduces to

$$X \sim \frac{E_f X_\mu}{E_d X_\mu + E_\mu}. \quad [\text{E3.13}]$$

The energy gain can be further maximized if

$$E_d X_\mu \gg E_\mu \quad [\text{E3.14}]$$

yielding

$$X \sim \frac{E_f}{E_d} \quad [E3.15]$$

with

$$N_\mu >> \frac{0.3 \phi^{\frac{2}{3}} r_o^3}{E_d X_\mu}$$

and

$$X_\mu >> \frac{E_\mu}{E_d}$$

Typical numbers of the variables for a 50-50 deuterium-tritium mixture are used to give a range of the energy gain and the number muons required to achieve such gains.

The 3.5 MeV α particle, created during μ dt or dt fusion, deposits all of its kinetic energy into the fuel. If there is sufficient fuel then the 14.1 MeV neutrons created may also deposit some of their kinetic energy into the fuel. The range of deposited energy into the fuel is

$$E_d = 3.5 \rightarrow 17.6 \text{ MeV} .$$

The energy cost of a muon in one muon production scheme is as low as 3000 MeV (24), however a more conservative value of 5000 MeV (2) is generally used, therefore

$$E_\mu = 3000 \rightarrow 5000 \text{ MeV} .$$

Using the above values the energy gain will have a range of

$$X = 1 \rightarrow 5 .$$

If the created neutron is used to breed fissile fuel from fertile fuel further energy can be extracted from the fusion event. If one fissile nuclei per fusion event is assumed then

$$X = 1 \rightarrow 60 .$$

In order to achieve the maximum values of the energy gain the muon efficiency must be

$$X_{\mu} > > 175 \rightarrow 1500 .$$

With these muon efficiencies, the range of required muons is

$$N_{\mu} > 10^{14} \rightarrow 10^{17} .$$

The above energy gains are small considering the fact that no efficiencies (e.g. energy conversion, muon production) are included in this analysis.

3.4 Ignition of standard fusion

Assuming that standard fusion dominates then standard fuel burnup will dominate in the numerator of Equation 3.10.

$$X = \frac{\frac{N_f}{2} E_f f_b}{0.3 \phi^{\frac{2}{3}} R_o^3 + N_{\mu} E_d X_{\mu} + N_{\mu} E_{\mu}} \quad [E3.16]$$

Heat generated by muon catalyzed fusion will need to be sufficient for the fuel to reach the ignition temperature, therefore

$$N_{\mu} E_d X_{\mu} \sim \frac{3}{2} N_f T_{\text{ign}} \quad [E3.17]$$

where T_{ign} is the ignition temperature of the fuel.

The minimum number muons required to initiate ignition is

$$N_{\mu} \sim \frac{\frac{3}{2} N_f T_{\text{ign}}}{E_d X_{\mu}} \quad [E3.18]$$

Once ignition is achieved the fuel will quickly heat to the maximum of the standard dt fusion cross-section, which is about 60 keV. At such a high temperature the disassembly time of the pellet will be very short. The fraction of fuel consumed can be formulated as (25)

$$f_b \sim \frac{1}{1 + \frac{2}{N \tau \sigma v}} \quad [E3.19]$$

with

N as the fuel density = $4.25 \times 10^{22} \phi$,

τ as the fuel disassembly time and

(σv) as the reaction crosssection.

The fuel disassembly time can be approximated by

$$\tau \sim \frac{r}{v_s} \quad [E3.20]$$

where r represents the radius of the spherical fuel pellet at the time of ignition. Assuming ignition occurs at some desired density, then

$$r = \frac{r_o}{\phi^{\frac{1}{3}}} \quad [E3.21]$$

where r_o is the initial radius.

The speed of sound can be approximated using

$$v_s \sim \left(\frac{2 T_b}{m_f} \right)^{\frac{1}{2}} \quad [E3.22]$$

where

$T_b = 60$ keV for 50 – 50 dt fuel and

m_f is the fuel atomic mass .

For dt fuel at $T_b = 60$ keV,

$$v_s \sim 2 \times 10^8 \left(\frac{\text{cm}}{\text{s}} \right),$$

and

$$(\sigma v) \sim 8.76 \times 10^{-16} \left(\frac{\text{cm}^3}{\text{s}} \right) \quad (24).$$

Using the above values, the expression for f_b can be reduced to

$$f_b \sim \frac{1}{1 + \frac{10.7}{r_o \phi^{\frac{2}{3}}}} \quad [E3.23]$$

Using the previous ranges of E_f , E_d and E_μ and using the following density range of

$$\phi = 1 \rightarrow 100$$

and assuming that the muon efficiency satisfies

$$X_\mu >> \frac{E_\mu}{E_d} = 175 \rightarrow 1500 \quad [E3.24]$$

then the energy gain can be written as

$$X \sim \frac{13617 E_f f_b}{0.3 \phi^{\frac{2}{3}} + 41 T_{\text{ign}}} \quad [E3.25]$$

The values of E_f and T_{ign} are in MeV and keV respectively. Using $E_f = 17.6$ MeV and $T_{\text{ign}} = 4$ keV and since the largest value of ϕ considered is 100, the maximum energy gain can be further reduced to

$$X \sim 133 r_o \phi^{\frac{2}{3}} \quad [E3.26]$$

This is achieved by reducing the burnup fraction to $f_b \sim (r_o \phi^{2/3})/10.4$. The fact that the density plays a role only in the burnup fraction means that most of the driver energy is required only to overcome the heat generated by the muon catalyzed fusion.

When the muon efficiency is not in the range

$$X_{\mu} < \frac{E_{\mu}}{E_d} = 175 \rightarrow 1500 ,$$

the energy gain depends primarily on the value of the muon efficiency and

$$X \sim X_{\mu} . \quad [E3.27]$$

The number of muons required to heat the fuel to ignition (for a 1 cm pellet) from Equation 3.18 is

$$N_{\mu} \sim \frac{(5 \times 10^{19} \rightarrow 2 \times 10^{21})}{X_{\mu}} . \quad [E3.28]$$

Assuming ideal conditions: a reaction time of 200 ns, pellet ignition, μdt and dt fusion only, no muon sticking or losses and reactions operating at the maximum muon cycling rate where the maximum value of X_{μ} is between 10^2 and 10^5 (see Figure 12 and Section 2.9) the energy gain could exceed 100. A 1 cm radius deuterium-tritium pellet is assumed in order that reasonable values of compression driver energy are used. Such a pellet would require at minimum 10^{15} muons in order to reach ignition. These muons would be required to be present in the pellet within a few muon cycling times of the start of the pellet compression. Since the muon cycling time is required to be high the muon pulse must be as short as possible, a few nanoseconds at the most. Ignition of standard fusion using heat generated by muon catalyzed fusion seems viable from these ideal, purely energetic arguments.

4. Power Balance Calculation

It was concluded in the Energy Gain Calculation in Section 3 that a large energy gain will result only if the fuel is brought to the ignition temperature of standard type fusion. If muon catalyzed fusion is used to ignite deuterium-tritium fuel a favourable power balance is also required.

The ignition temperature of the fusion fuel is a temperature where the power gained by the fuel through fuel compression and fuel heating from fusion reaction products (boot-strap) exceeds the power losses from all sources. Here it is considered that fuel heating will come primarily from the deposited energy of energetic fusion by-products from both muon catalyzed fusion and standard fusion. Bremsstrahlung radiation is the primary mechanism of power loss during compression and will be the only loss mechanism considered.

The following analytic formula can be used to calculate the standard fusion power versus temperature and density for a 50-50 deuterium- tritium fuel (26) and is

$$P_{SF} = 2.28 \times 10^{17} e^{-0.47 \left| \log\left(\frac{T_{eV}}{69000}\right) \right|^{2.25}} \phi^2 \left(\frac{W}{cm^3}\right). \quad [E4.1]$$

The Bremsstrahlung losses can be calculated with the following formula (27),

$$P_{Br} = 3.10 \times 10^{13} \sqrt{T_{eV}} \phi^2 \left(\frac{W}{cm^3}\right). \quad [E4.2]$$

The point at which the boot-strap standard fusion power exceeds the Bremsstrahlung losses for a small (1 cm) spherical d-t pellet is approximately 4.0 keV (see Figure 15). If a large enough pellet were used, a certain amount of the Bremsstrahlung radiation could be reabsorbed by the fuel and not lost from the system. In order to calculate this, the mean free path of the emitted radiation must be known for the range of temperature and densities of interest. The mean free path can be calculated as

$$l_{mfp} \sim \frac{1}{0.224 \phi \kappa_r} \text{ (cm)} \quad [E4.3]$$

where κ_r is the Rosseland opacity.

Using tabulated values of the temperature and density dependent Rosseland opacity (28), the mean free path of emitted radiation and reabsorption factor can be calculated. Only a shell of one mean free path deep from the surface of the fuel body is considered to radiate out the Bremsstrahlung radiation. The effective power loss is then a fraction of the Bremsstrahlung power loss in Equation 4.2. The reabsorption factor is related to the geometry, the mean free path of radiation and the radius at a given temperature and density. For spherical geometry the factor of Bremsstrahlung radiated out or lost is,

$$f_{\text{sph}} = 3 \left(\frac{l_{\text{mfp}}}{r} \right) - 3 \left(\frac{l_{\text{mfp}}}{r} \right)^2 + \left(\frac{l_{\text{mfp}}}{r} \right)^3, \quad \text{for } \frac{l_{\text{mfp}}}{r} < 1 \quad [\text{E4.4}]$$

$$f_{\text{sph}} = 1, \quad \text{for } \frac{l_{\text{mfp}}}{r} > 1$$

with

$$r = \frac{r_0}{\phi^{\frac{1}{3}}}$$

where r_0 is the initial radius of the pellet.

Figure 15 plots the ignition temperature (where standard fusion gains equal effective Bremsstrahlung losses) versus fuel density for pellets of initial radius from 1 cm to 5 cm. It is concluded from Figure 15 that unless the fuel pellet is very big the ignition temperature is around 4 keV for densities less than 100. Very large pellets will lead to unacceptable muon costs and compression driver energy costs, therefore the Bremsstrahlung power losses can be represented by Equation 4.2.

The muon catalyzed fusion power deposited into the fuel pellet during compression can be represented by

$$P_{\mu\text{CF}} = \lambda_c N_\mu E_d \phi \left(\frac{W}{\text{cm}^3} \right). \quad [\text{E4.5}]$$

Muon decay is ignored in Equation 4.5, it is assumed that the reaction time is much shorter than the muon lifetime. The standard fusion power gains, the Bremsstrahlung power losses and the muon catalyzed fusion gains are all plotted for densities, $\phi = 1, 5, 10, 50, 100$, in Figures 16 to 20 respectively.

Looking over Figures 16 to 20, it is evident that a power gap exists between muon catalyzed fusion generated power and the power required to ignite standard deuterium-tritium fusion. This power gap suggests that muon catalyzed fusion cannot be used to ignite deuterium-tritium fuel, however the power balance analysis ignores the dynamical (spatial) nature of the fuel compression. It is possible that some part of the fuel may be 'sparked' (ignited) and generate sufficient energy to ignite the surrounding fuel. A simulation of the spatial dynamics of deuterium-tritium fuel compression with muons is required to see if the spark effect arises. A spatial compression simulation is performed in Section 5.

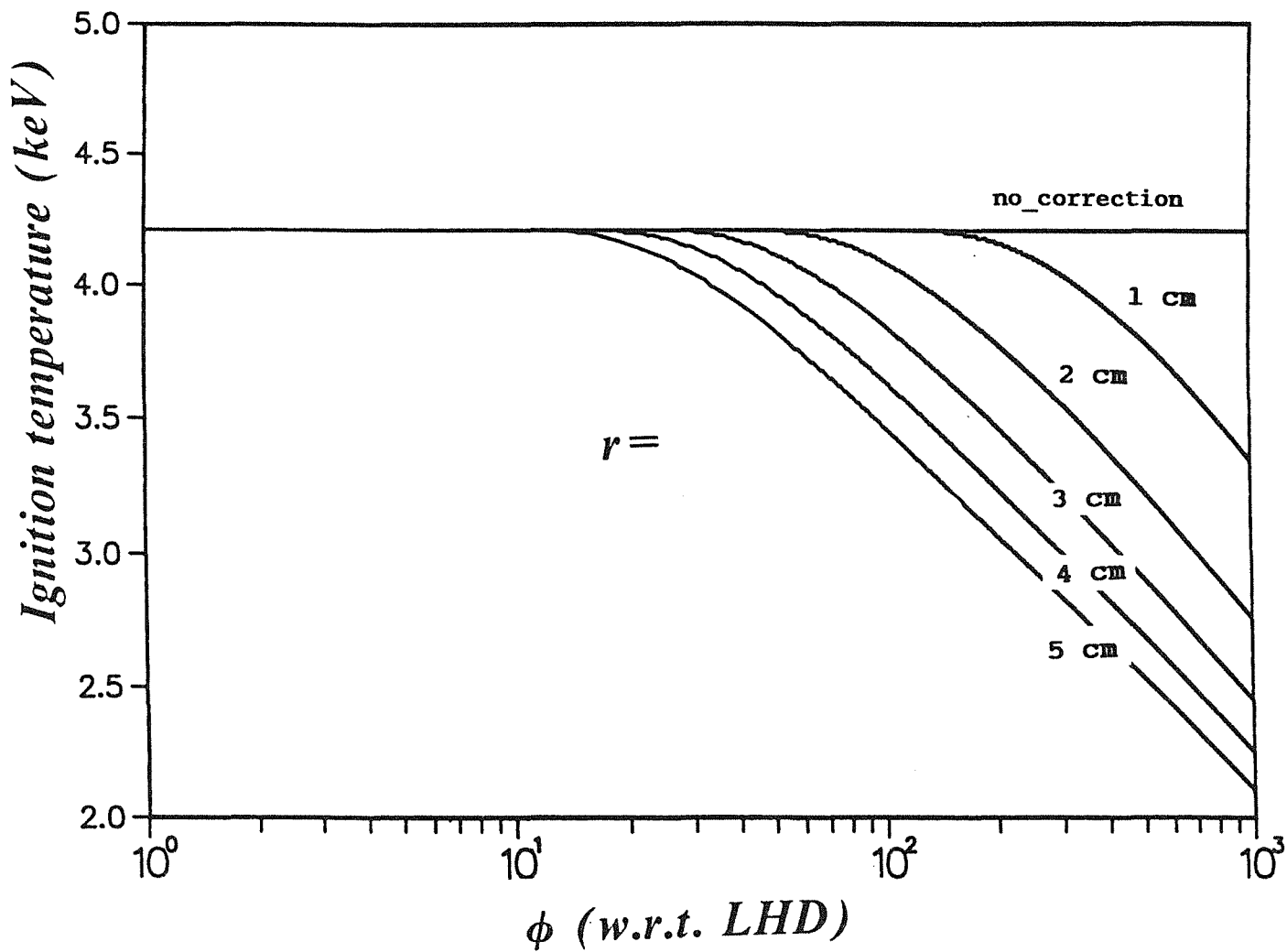


Figure 15

The ignition temperature of 50%-50% deuterium-tritium spherical fuel pellets of various radii. The no-correction case means that there is no re-absorption correction applied to the Bremsstrahlung losses.

$$\phi = 1$$

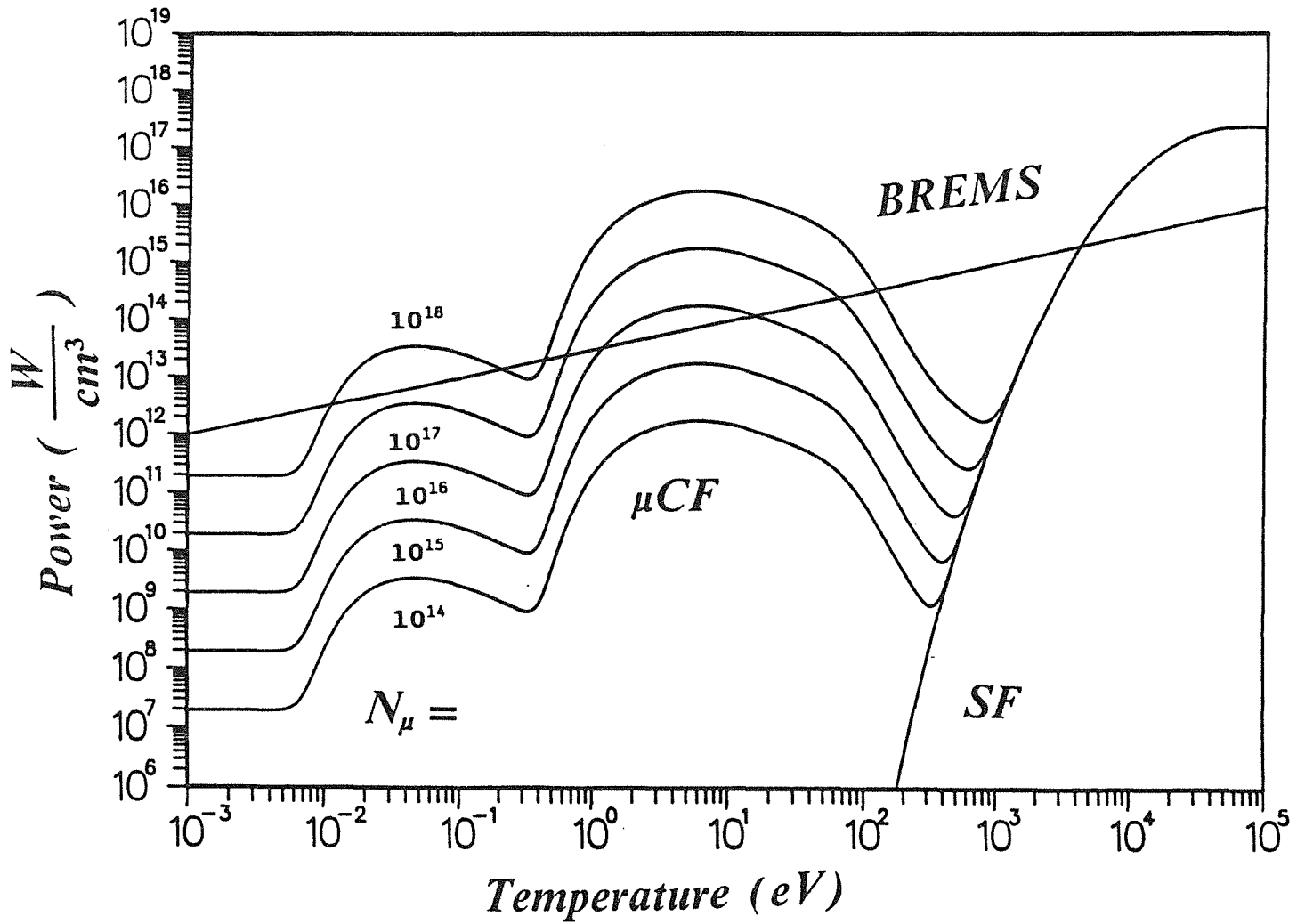


Figure 16

Power balance for a 1 cm radius, 50%-50% deuterium-tritium spherical fuel pellet compressed to a density of 1 with respect to LHD.

μCF represents power generated by muon catalyzed fusion reactions.

SF represents power generated by standard fusion reactions.

BREMS represents power losses due to Bremsstrahlung.

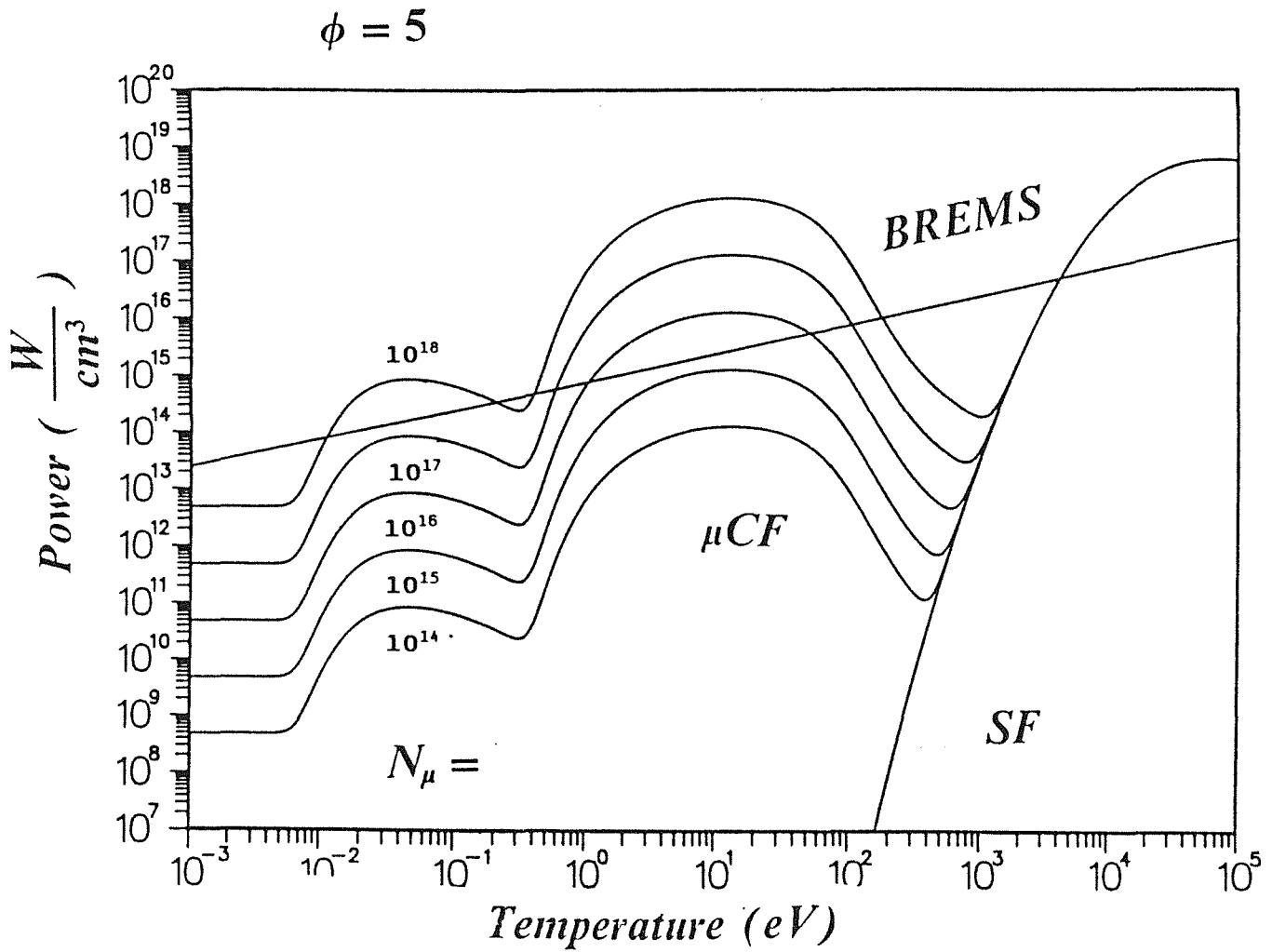


Figure 17

Power balance for a 1 cm radius, 50%-50% deuterium-tritium spherical fuel pellet compressed to a density of 5 with respect to LHD.

μCF represents power generated by muon catalyzed fusion reactions.

SF represents power generated by standard fusion reactions.

BREMS represents power losses due to Bremsstrahlung.

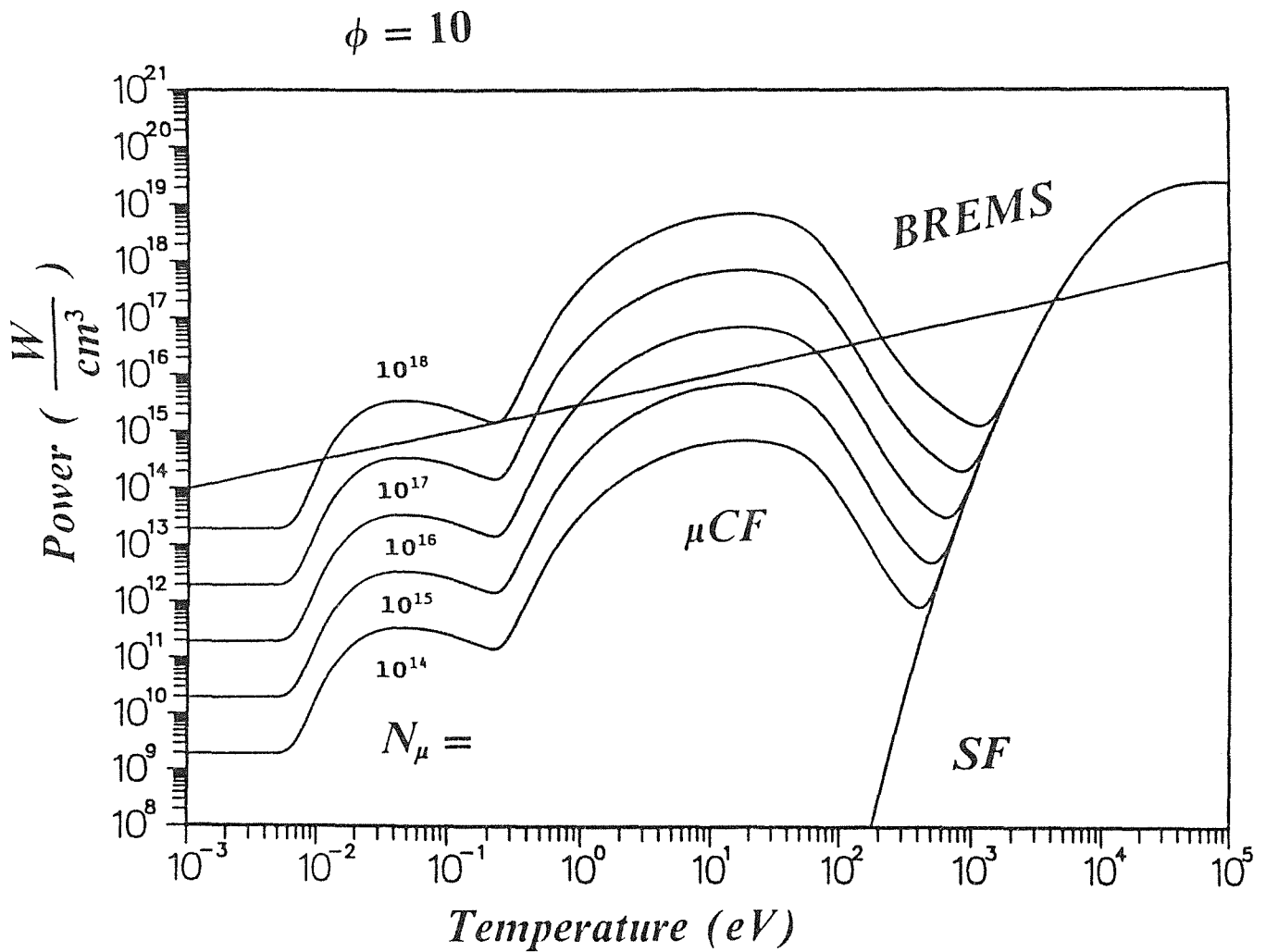


Figure 18

Power balance for a 1 cm radius, 50%-50% deuterium-tritium spherical fuel pellet compressed to a density of 10 with respect to LHD.

μCF represents power generated by muon catalyzed fusion reactions.

SF represents power generated by standard fusion reactions.

BREMS represents power losses due to Bremsstrahlung.

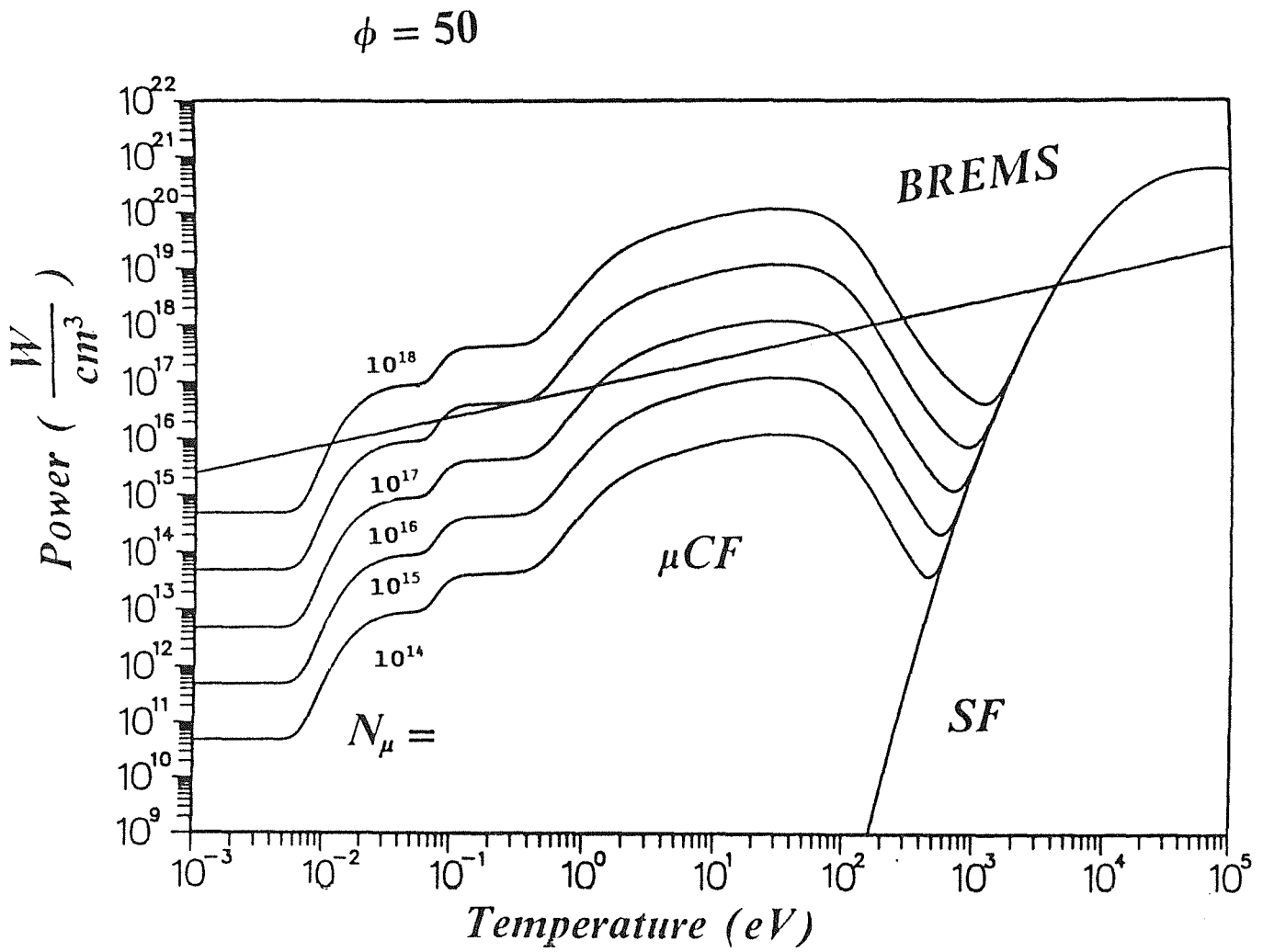


Figure 19

Power balance for a 1 cm radius, 50%-50% deuterium-tritium spherical fuel pellet compressed to a density of 50 with respect to LHD.

μCF represents power generated by muon catalyzed fusion reactions.

SF represents power generated by standard fusion reactions.

$BREMS$ represents power losses due to Bremsstrahlung.

$$\phi = 100$$

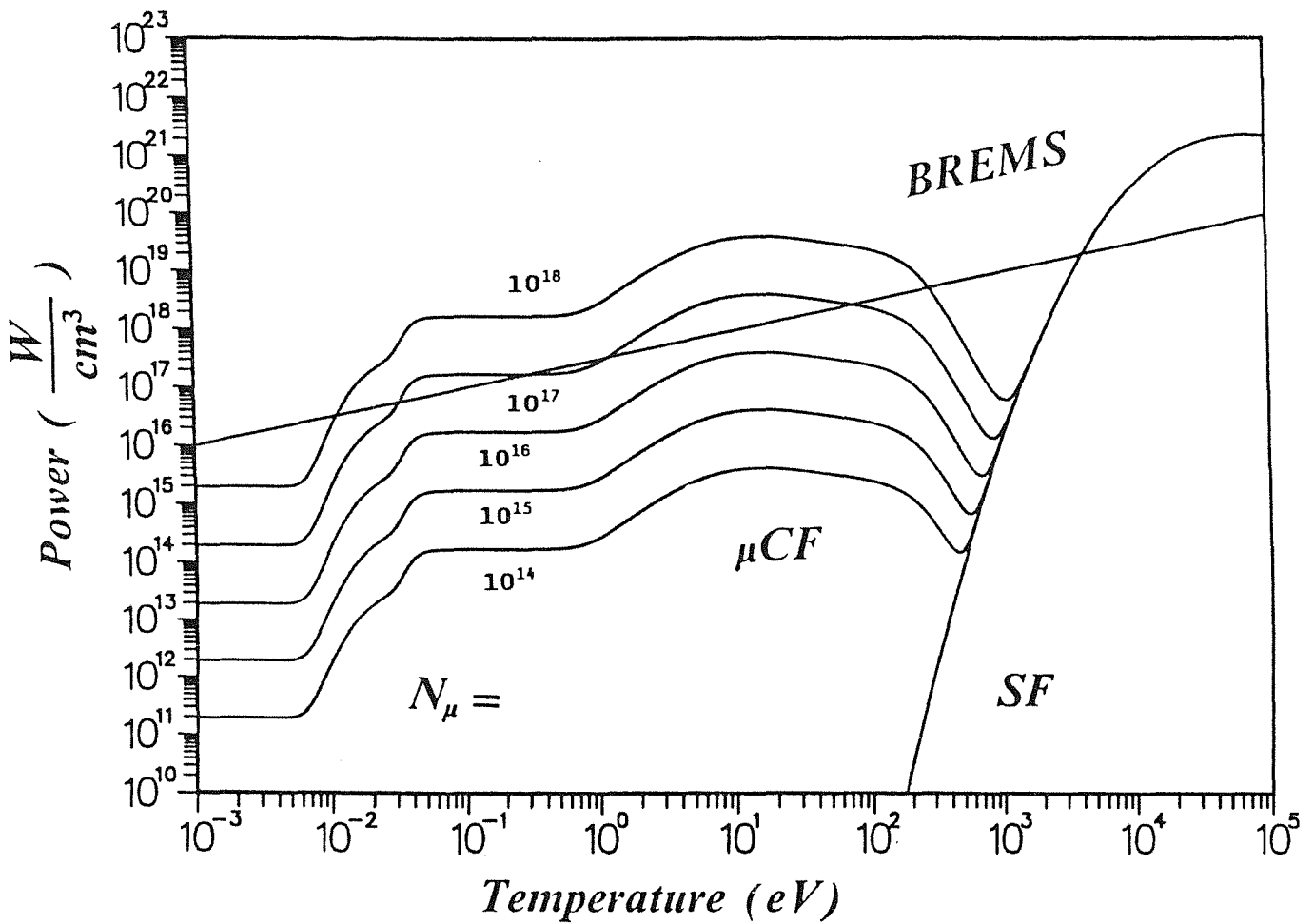


Figure 20

Power balance for a 1 cm radius, 50%-50% deuterium-tritium spherical fuel pellet compressed to a density of 100 with respect to LHD.

μCF represents power generated by muon catalyzed fusion reactions.

SF represents power generated by standard fusion reactions.

BREMS represents power losses due to Bremsstrahlung.

5. Muon catalyzed fusion under compression

It is clear that an external force will be required to counteract the pressure generated by muon catalyzed fusion in a deuterium-tritium pellet. It is desirable to generate high densities in the fuel since the muon catalyzed fusion reaction rates become larger and ignition at high densities yield high energy gains (see Equation 3.19). In order to compress a spherical pellet a series of shock waves are created at the pellet surface timed such that they coalesce near the center of the pellet. In traditional Inertial Confinement Fusion schemes the deuterium-tritium fuel is hopefully sparked at this coalescence and the density is such that a burning wave generates a high energy gain. In order to achieve the maximum density increase in a pellet with minimum of external driver energy a series of converging shocks are created at the pellet surface such that they will not overtake each other before they reach the pellet center. In the isentropic case the prescribed pressure pulse shape at the pellet surface is (25)

$$P(r,t) = P_0 \left(1 - \frac{t}{t_c}\right)^{-\frac{5}{2}} \quad [E5.1]$$

where P_0 is the initial pressure at the pellet surface and t_c is the compression time.

The main condition of the isentropic approximation is minimal heating during compression (29), however if muons are present in the fuel, heating will occur due to muon catalyzed fusion reactions. The pressure pulse required to compress the pellet will then depend upon the rate of heating within the pellet which in turn depends upon the local temperature and density. This non-linear dependence is not easily resolved and small changes in the muon catalyzed fusion cross-sections may have large consequences on the pressure pulse needed and the final energy gain.

At the last moment of the pressure pulse the pellet should be near ignition. Assuming that the whole fuel pellet is near the ignition temperature (use 4 keV) then the pressure pulse should equal the internal pressure of the pellet which will be 54000 GPa. The time required for the created shock to reach the center of the pellet can be calculated with (29)

$$t_c = \left(\frac{P_s}{m n}\right)^{\frac{1}{2}} \quad [E5.2]$$

where

P_s is the pressure generated at pellet surface ,

m is the mass (for 50 – 50 dt) = 4.18×10^{-27} kg and

n is the density = $4.25 \times 10^{22} \phi \text{ cm}^{-3}$.

If a constant pressure pulse of 54000 GPa were used the compression time would be about 20 ns for an initial pellet radius of 1 cm. This time is too small for any reasonable number of muon catalyzed fusion reactions to occur. Also with a constant pressure the maximum density increase that can be expected is 4 (30).

The isentropic case can be used for a first approximation and may yield some insight into resolving the problem of non-linearity. Using the isentropic pressure pulse in Equation 5.1 and the fact that the pressure pulse can be applied at best for 90 % of the compression time, the initial pressure is $P_0 \sim 850$ GPa . For an isentropic pulse a primary consequence is that any shocks created will not overtake the initial shock, therefore the compression time is calculated with the initial pressure applied to the pellet. Using Equation 5.2 and a pellet radius of 1 cm, the compression time $t_c = 130$ ns and the time period that the pressure will be applied is 117 ns. Figure 21 shows such a pressure pulse.

The pressure pulse will be applied to the surface of the pellet and the energy required to generate the desired final densities will be proportional to the surface area of the pellet. With a pellet radius of 1 cm the driver power required will be in the range of 100 TW. Such a driver power is possible (24), however such high powers for 100-200 ns may be unattainable.

The one dimensional Lagrangian simulation code, KATACO (KAlsruhe TARget COde) was modified to include muon catalyzed fusion reactions (see Appendix A). The code was used to simulate only deuterium-tritium standard reactions and μ dt muon catalyzed fusion reactions. The simulation requires an input pressure pulse and an initial muon concentration. Simulations were performed using the pressure pulse in Figure 21 and initial muon concentrations of 10^{14} , 10^{15} , 10^{16} and 10^{17} cm^{-3} and also the no-muon case.

It was assumed in the following calculations that the muon sticking is zero so that the best possible case arises. With this condition the minimum number of muons required to ignite a dt pellet of reasonable size will come to light. If the number of muons required is unreasonable for the no-sticking case then this fusion scheme will be more unattractive when muon sticking is included in the calculations.

The time evolution of the pellet radius, the pellet surface velocity, the energy gain due to the standard dt fusion, the energy gain due to μ dt muon catalyzed fusion, the total energy gain and the total energy output are calculated and may be displayed during a simulation run.

The time history of the radius of the pellet assuming the isentropic case is (29)

$$r(t) = r_0 \left(1 - \frac{t}{t_c}\right)^{\frac{1}{2}} . \quad [E5.3]$$

The time evolution of the pellet radii from the computer simulation with various initial muon concentrations are plotted in Figure 22. The no-muon case appears to follow the anticipated curve of Equation 5.3 until near the end of the compression time where the pellet quickly disassembles. With larger initial muon concentrations, the radius history of the pellet resembles more to the initial pellet radius. This is due to the increased energy inside the pellet working against the externally applied pressure. As expected, the disassembly is more

violent as the muon concentration increases due to the increased energy released into the pellet.

For initial muon concentrations greater than about 10^{17} cm^{-3} the simulation will not work in its present state. This is likely due to large differences in the temperature and density profiles of the pellet since muon catalyzed fusion heating becomes very large.

The velocity at which the surface of the pellet moves for the isentropic approximation can be calculated by differentiating the radius equation (see Equation 5.3) which yields

$$u(t) = -\frac{r_o}{t_c} \frac{\frac{t}{t_c}}{\left(1 - \frac{t}{t_c}\right)^{\frac{1}{2}}} \quad [E5.4]$$

Figure 23 plots the time evolution of the pellet surface velocity for various initial muon concentrations including the no-muon case. The no-muon case follows the Equation 5.4 prior to disassembly closely. When muons are present the pellet's surface velocity is slowed during the compression time and becomes highly erratic when the initial muon concentration is 10^{17} cm^{-3} . At about 120 ns the pellet disassembles for all cases and the velocity of the pellet reverses. For the initial muon concentration of 10^{17} cm^{-3} the post-compression velocity is very large indicating successful ignition.

The energy gain due only to standard fusion, only to muon catalyzed fusion and the total fusion yield are plotted for various initial muon concentrations in Figures 24, 25 and 26 respectively. The energy gain or yield is defined as the total energy out divided by the total energy in. The energy out is due only to standard dt fusion in Figure 24, due only to μdt muon catalyzed fusion in Figure 25 and both are combined in Figure 26. The energy in is calculated from both compression and muon energy costs for all energy gain calculations. In Figure 24 it is seen that only with an initial muon concentration of 10^{17} cm^{-3} the pellet is properly ignited. Figure 25 shows the surprising result that as the initial muon concentration increases the energy gain decreases. This is due to the pellet being hotter for higher muon concentrations where the muon catalyzed fusion reaction rates decrease for higher temperatures (see Figure 14). The earlier conclusion that the yield due to only muon catalyzed fusion approaches some limiting value below 5 (see Section 3.3, Energy gain dominated by muon catalyzed fusion) is not confirmed. The initial muon concentration of 10^{14} cm^{-3} yields a value of around 10. This could be due to the inclusion of the dynamical behaviour of the fuel compression inherent in the simulation. The total energy gain is plotted in Figure 26. For an initial muon concentration of 10^{17} cm^{-1} , the high energy gain (Figure 26) and the violence of disassembly (Figure 22) suggests that the pellet is ignited. The probable cause of ignition is 'sparking' by a hot region where the temperature exceeds 4 keV. The total energy gain is in accordance with that found in Section 3.4, Ignition of standard fusion. The total energy out is also plotted in Figure 27 to gain an insight on the magnitude of the energy generated.

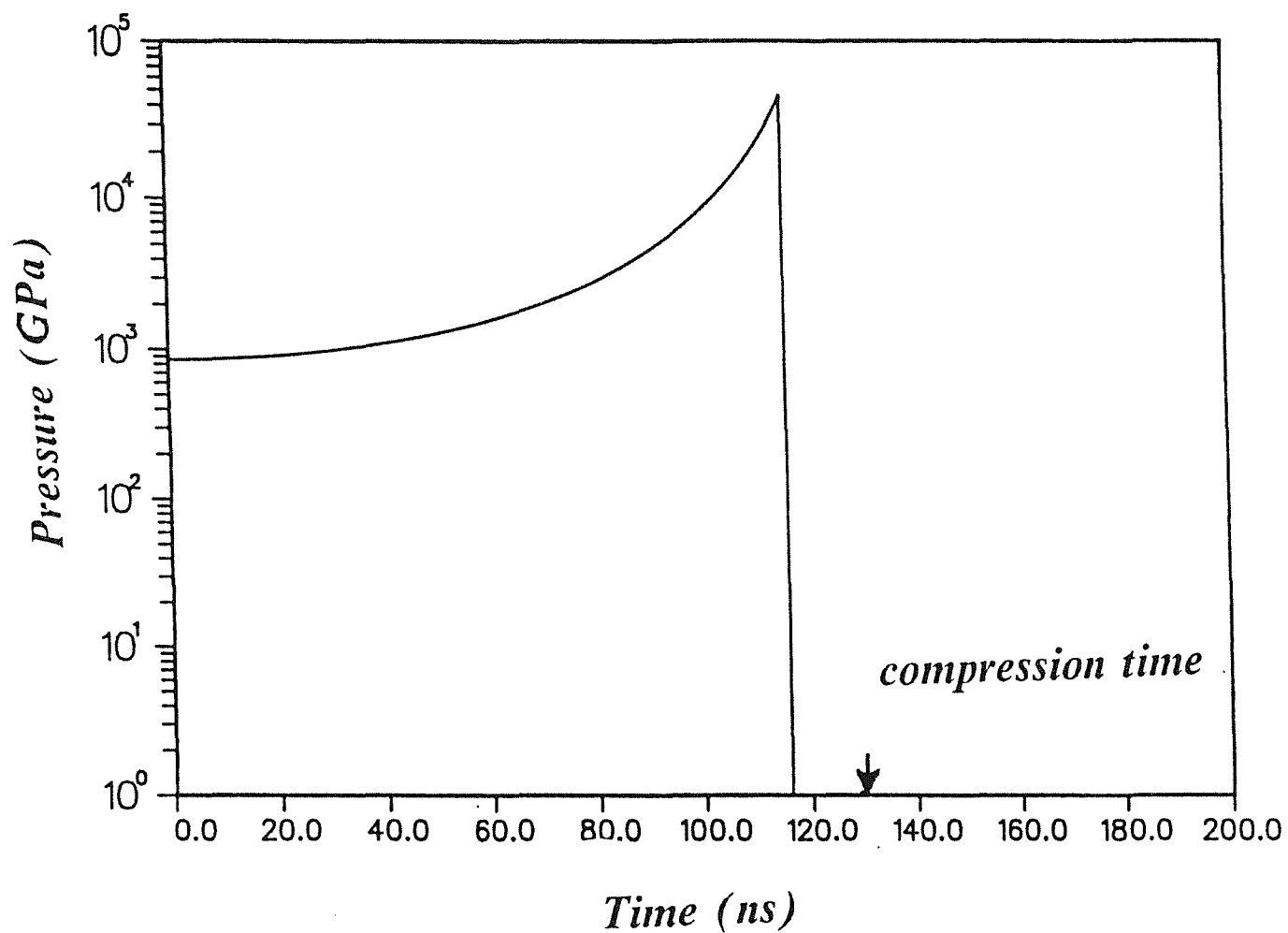


Figure 21

Pressure pulse applied to surface of the pellet. The pressure pulse, in the isentropic approximation, is 90% of the compression time.

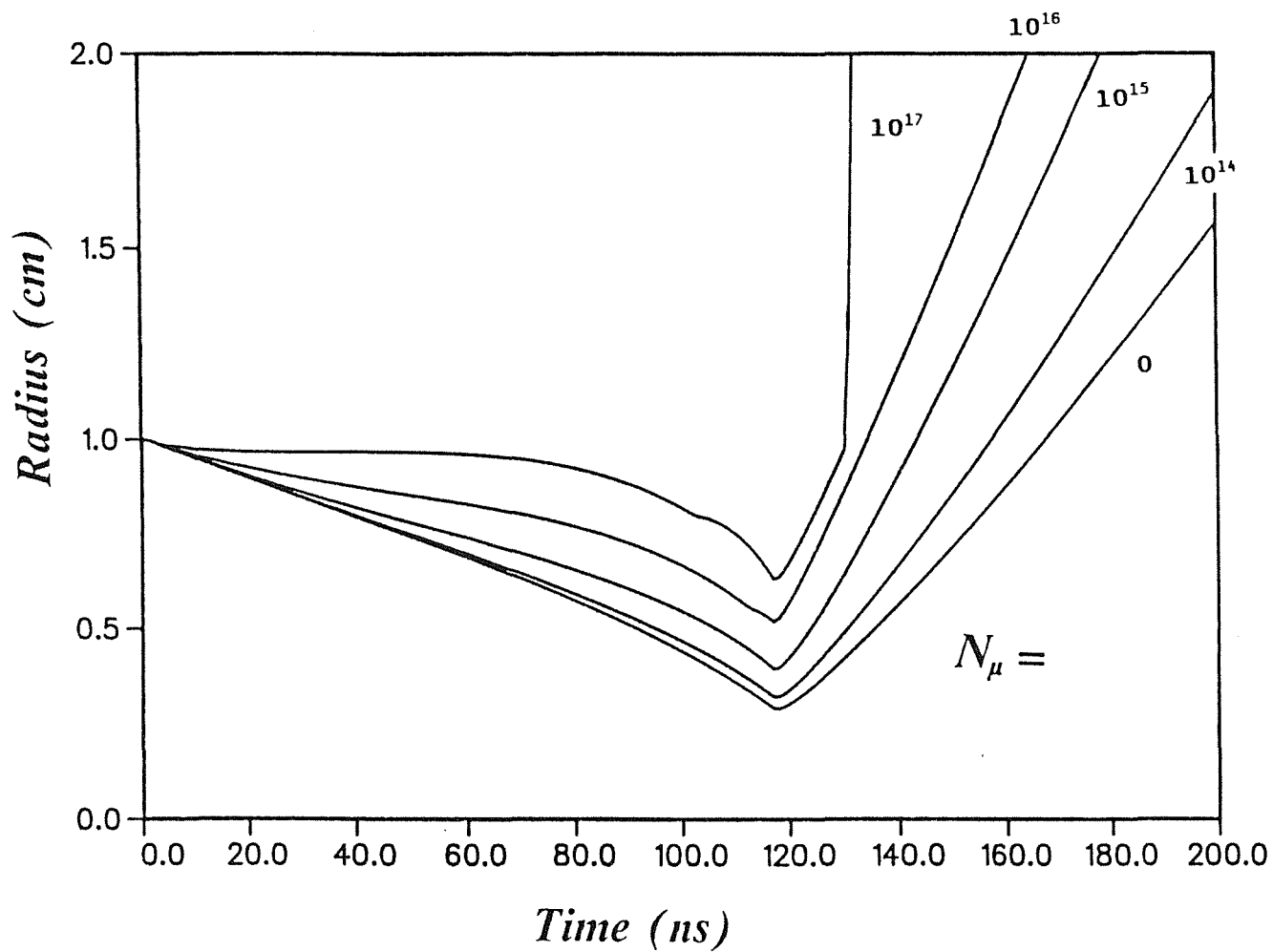


Figure 22

The time evolution of the radius of an initially 1 cm radius pellet when the pressure pulse in figure 21 is applied for various initial muon concentrations.

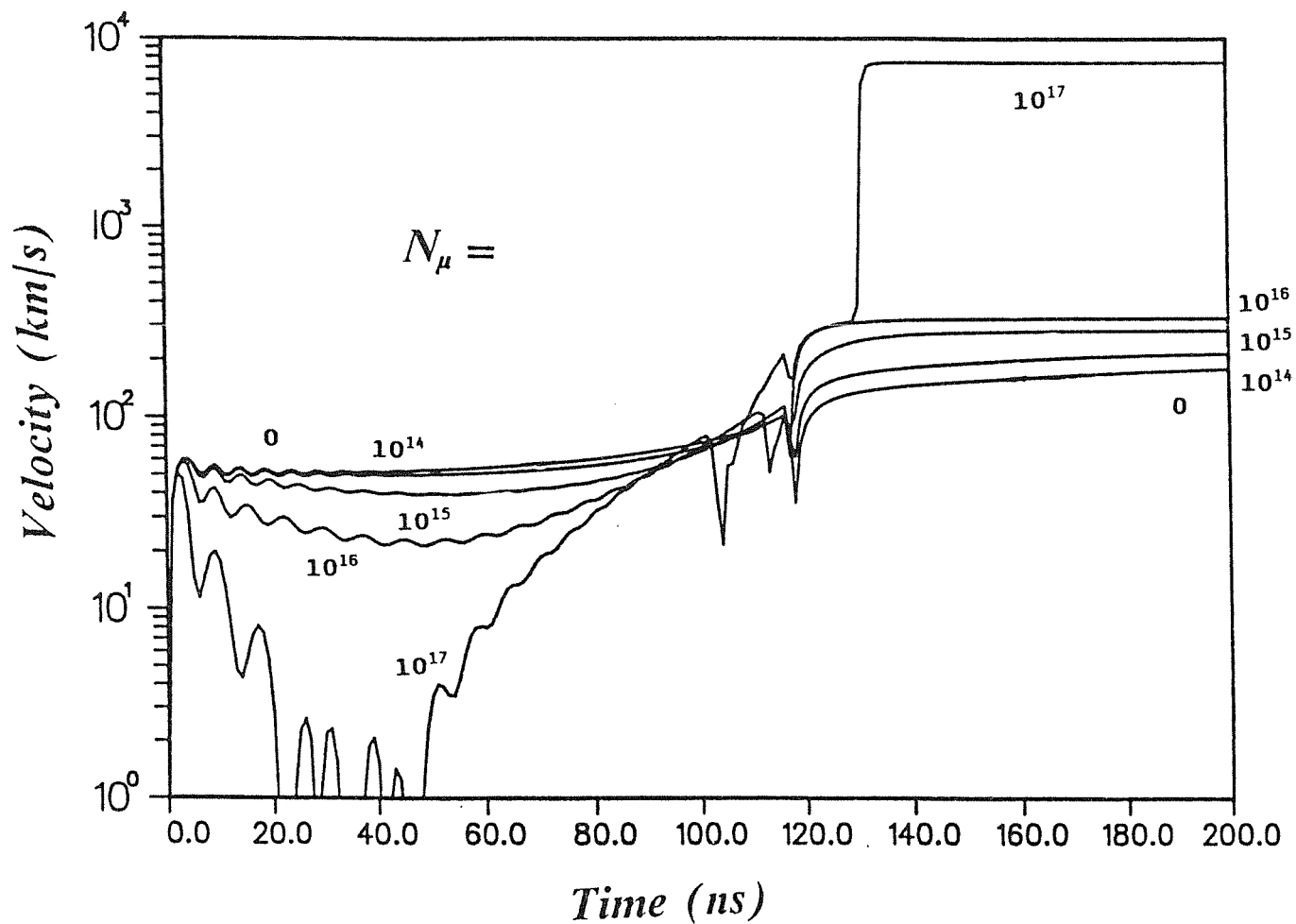


Figure 23

The time evolution of the pellet surface velocity of an initially 1 cm radius pellet when the pressure pulse in Figure 21 is applied for various initial muon concentrations. Note: The pellet disassembly causes a change in the sign of the velocity, however the absolute value of the velocity is plotted here.

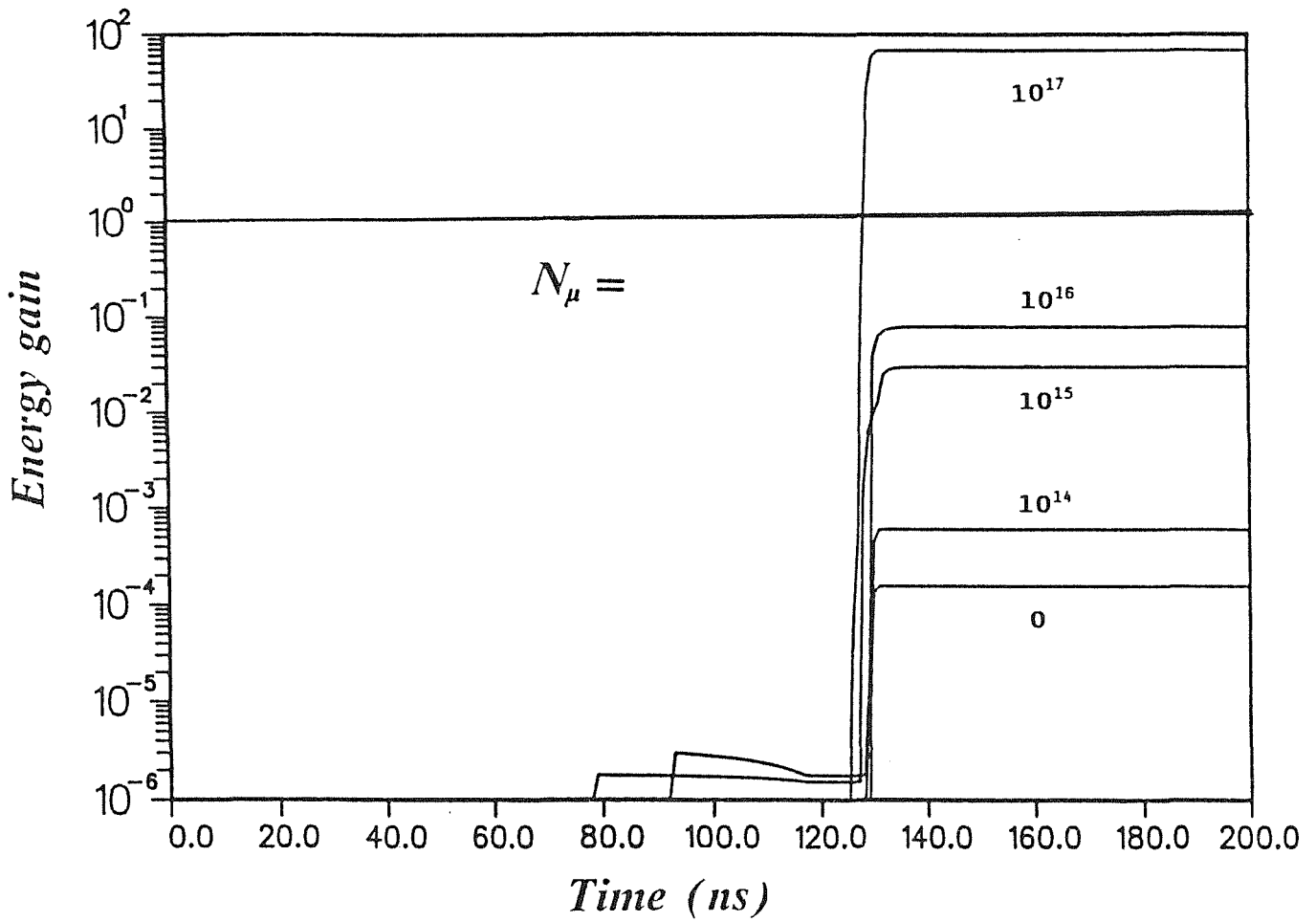


Figure 24

The energy gain due only to standard type dt fusion reactions for a 1 cm radius, 50%-50% deuterium-tritium spherical fuel pellet compressed by the pressure pulse in figure 21 for various muon concentrations.

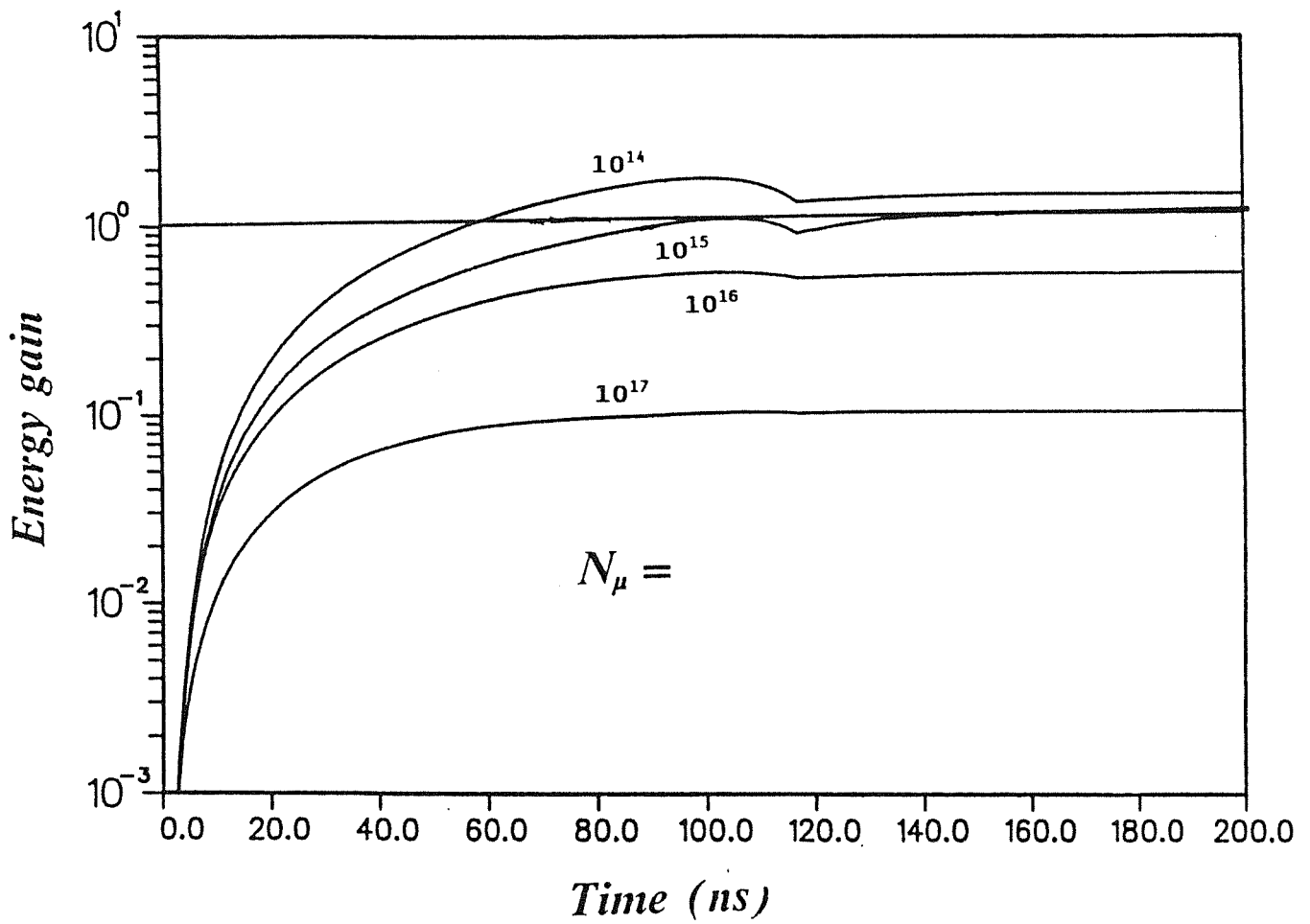


Figure 25

The energy gain due only to muon catalyzed μdt fusion reactions for a 1 cm radius, 50%-50% deuterium-tritium spherical fuel pellet compressed by the pressure pulse in figure 21 for various muon concentrations.

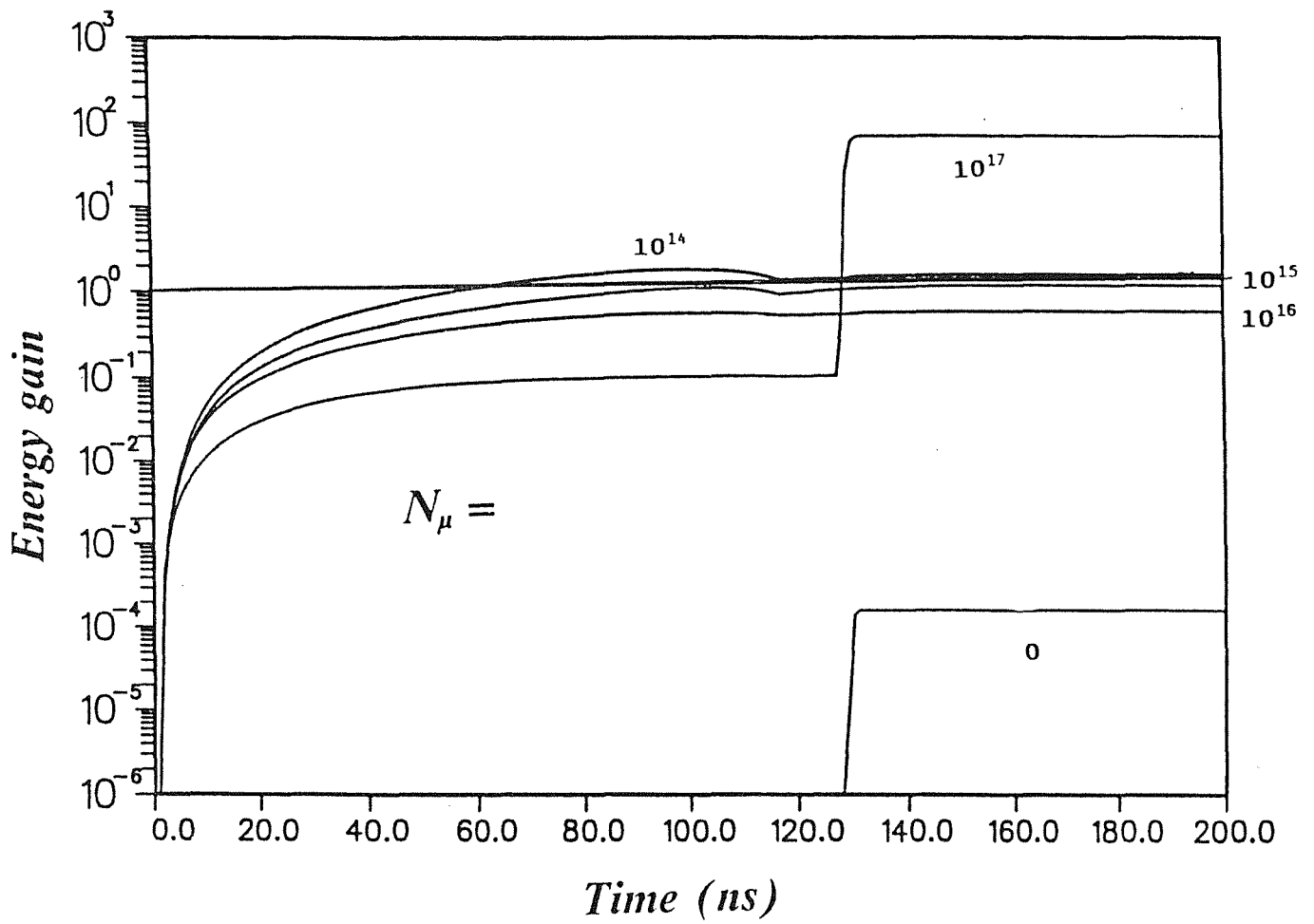


Figure 26

The energy gain due to muon catalyzed μ dt fusion and standard dt fusion reactions for a 1 cm radius, 50%-50% deuterium-tritium spherical fuel pellet compressed by the pressure pulse in figure 21 for various muon concentrations.

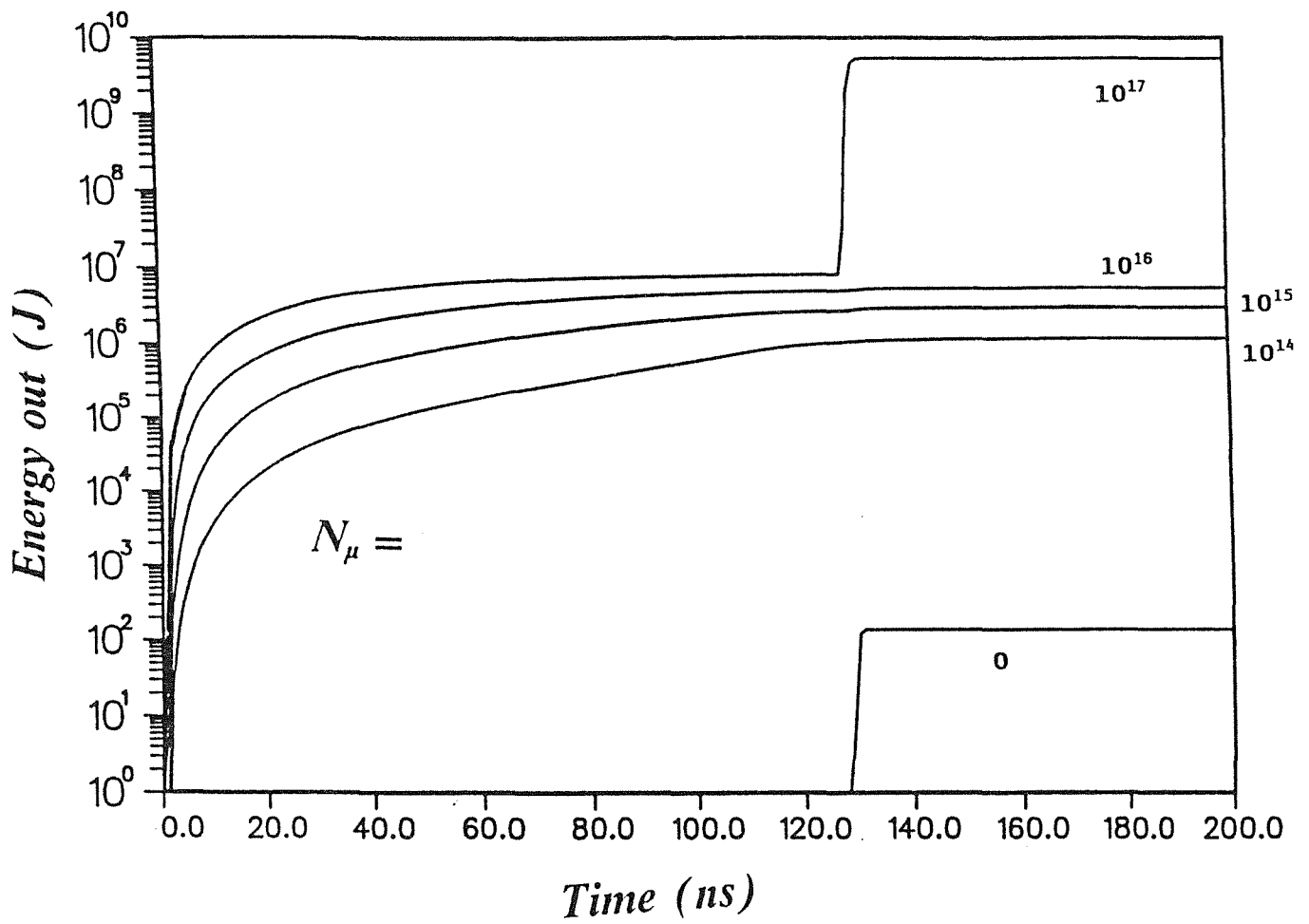


Figure 27

The total energy output due to muon catalyzed μ dt fusion and standard dt fusion reactions for a 1 cm radius, 50%-50% deuterium-tritium spherical fuel pellet compressed by the pressure pulse in figure 21 for various muon concentrations.

6. Discussion

Theoretical and computational investigations of Muon Catalyzed Fusion of 50/50 deuterium-tritium fuel pellets under compressive conditions were reported here. The initial idea was to combine the two current fusion technologies, Muon Catalyzed Fusion and compression driven fusion (i.e. Inertial Confinement Fusion) to see if there was a complementary or symbiotic relationship. The most difficult though most important task was to formulate the various muon catalyzed fusion reaction rates at a range of temperatures and densities found in highly compressed matter. Section 2 attempted to find 'order of magnitude' values of the reaction rates, however some important points were left out. They include the back decay of the muo-molecular ion which will reduce the effective muo-molecular formation rate, and the muo-atomic spin states which may increase or decrease (depending on the spin states which are preferentially populated) the formation rate of muo-molecules. Once all the muon catalyzed fusion reaction rates were formulated an effective cycling rate was devised which yields a simplified model of the muon catalyzed fusion processes. This approach significantly reduced the computation effort since the full set of kinetic equations is reduced to one equation. This approach may breakdown in a computer simulation if the local density and temperature change faster than the muon catalyzed fusion reaction rates, then the full set of kinetic equations must be solved at each time step. The muon sticking question was not fully discussed but it was stated early that the no-sticking case would be primarily used. If the no-sticking case doesn't yield positive results, they would further deteriorate with any kind of sticking.

In a simple energy balance calculation of the combined system it was found that the fuel must be ignited to standard fusion temperature for significant energy gain. Computer simulations in Section 5 confirm this calculation. The focus of the report then became the question, 'How many muons and what magnitude of compression driver are required to ignite a dt pellet?'

Power balance calculations in Section 4 showed that it may not be possible to ignite a 1 cm radius dt pellet. The conclusion was that muon catalyzed fusion reactions could not deliver sufficient power near the ignition point of standard dt fusion. This calculation ignored dynamical effects in a compressing pellet that may spark standard dt fusion.

The results of simulation of a compressing dt pellet with muons suggest that sparking of standard dt fusion occurs for a muon concentration of 10^{17} cm^{-3} in a 1 cm radius, 50-50 dt pellet under 'ideal' conditions (e.g. all muons are present initially, no muon sticking, etc.). The number of muons required to create a concentration of 10^{17} cm^{-3} is enormous by today's standards. Current muon factories can deliver 10^6 muons in a pulse (31). Current speculative schemes to produce muon pulses could deliver perhaps 10^{12} muons (32). Of these produced muons only about one hundredth would be stopped in a 1 cm radius dt pellet (see Section 2.3, Muon stopping). Included are problems of focussing high energy muon beams and inevitable muon losses during transfer. In order for our idealized muon catalyzed fusion ignition scheme to work a pulse of more than 10^{20} muons are required. A more abundant source of muons is clearly required for this scheme to work.

'If it is a rose, it will bloom'.

Acknowledgements

G. Cripps thanks Prof. G. Keßler, Dr. R. Fröhlich and Dr. B. Goel for making the opportunity for his stay at INR and to the DAAD for funding it.

7. References

1. S.S. Gershtein and L.I. Ponomarev, *Phys. Lett.*, 72B, 80 (1977).
2. Yu. Petrov, *Nature*, 285, 466 (1980).
3. S.E. Jones et al., *Phys. Rev. Lett.*, 56, 588 (1986).
4. Yu. Petrov, *Muon catalyzed Fusion* 1, p. 351 (1987).
5. S.E. Jones, 'Survey of Experimental Results in Muon Catalyzed Fusion', AIP Conf. 181, *Muon Catalyzed Fusion*, eds. S.E. Jones, J. Rafelski and H.J. Monkhorst, Sanibel Island, FL, p. 2 - 16 (1988).
6. A.A. Harms, G. Cripps and B. Goel, 'Energy Gain of ICF- μ CF Symbiosis', Proc. of the Fifth International Conference on Emerging Nuclear Energy Systems (ICENES) 1989, Karlsruhe, FRG, eds. U von Moellendorff and B. Goel, Word Scientific Publishing, p. 267 - 270.
7. G. Herzberg, *Molecular Spectra and Molecular Structure* 1, Second Edition, D. Van Nostrand Co., NJ (1959).
8. C.A. Rouse, 'Calculation of Stellar Structure', Appendix A, *Progress in High Temperature Physics and Chemistry*, ed. C.A. Rouse, Pergamon Press (1971).
9. R.M. More, 'Atomic Physics in Inertial Confinement Fusion', Lawrence Livermore Laboratory Preprint, UCRL-84991 Part I and II (1981).
10. A. Kumar and S. Sahin, 'Potential of Muon Catalyzed Fusion-Fission (Hybrid) Reactors', *Alternative Energy Sources V, Part E - Nuclear/ Conservation/ Environment*, ed. T.N. Veziroglu, Elsevier Science Publishers B.V., Amsterdam (1983).
11. H. Takahashi et al., *Atomenergie*, Vol. 36, No. 3, p. 593 (1961).
12. B. Goel, G.A. Moses, and R. Peterson, *Laser and Particle Beams*, 5, p. 133 (1987).
13. A.S. Wrightman, *Phys. Rev.*, Vol. 77, No. 4 (1950).
14. S. Eliezer, 'Muon Catalyzed Fusion for Energy Production', *Muon Catalyzed Fusion and Fusion with Polarized Nuclei*, eds. B. Brunelli and G.G. Leotta, Plenum Press, p. 19 - 53 (1987).
15. A.M. Lane, 'Theory of Cross-section for Formation of Meso-molecules', *Muon Catalyzed Fusion and Fusion with Polarized Nuclei*, eds. B. Brunelli and G.G. Leotta, Plenum Press, p. 55 - 66 (1987).
16. A.M. Lane, 'A Direct Process for Meso-molecular Formation at High Temperatures', AIP Conf. 1981, *Muon Catalyzed Fusion*, eds. S.E. Jones, J. Rafelski and H.J. Monkhorst, Sanibel Island, Fl, p. 226 - 235 (1988).
17. L.I. Men'shikov and L.I. Ponomarev, *JETP Lett.*, Vol. 46, No. 6, p. 312 - 315, 25 September 1987.

References (cont.)

18. G. Fiorentini, 'Muon Catalyzed Fusion: A Short Introduction and a Few Comments', Muon Catalyzed Fusion and Fusion with Polarized Nuclei, eds. B. Brunelli and G.G. Leotta, Plenum Press, p. 9 - 17 (1987).
19. L. Bracci and G. Fiorentini, Nature, Vol. 297, p. 135 - 136, 13 May 1982.
20. S.S. Gershtein et al., Sov. Phys. JETP, 51(6), 1053, June 1980.
21. S.G. Lie and A.A. Harms, Nuclear Science and Engineering: 80, p. 124 - 129 (1982).
22. D.V. Balin et al., Phys. Lett 141B, p. 173 (1984).
23. W. Seifritz and B. Goel, Atomenergie-Kerntechnik, Vol. 43, No. 3, p. 198 - 202 (1983).
24. G.R. Shin and J. Rafelski, 'Double Target Option for Pion Production for Muon Catalyzed Fusion', Proc. of the Fifth International Conference on Emerging Nuclear Energy Systems (ICENES) 1989, Karlsruhe, FRG, eds. U. von Möllendorff and B. Goel, World Scientific Publishing, p. 271 - 275.
25. J.J. Duderstadt and G.A. Moses, Inertial Confinement Fusion, J. Wiley and Sons (1982).
26. B. Brunelli, Nuovo Cimento 55, p. 264 (1980).
27. T. Kammash, Fusion Reactor Physics: principles and technology, Ann Arbor Sciences Publishing, Ann Arbor, Mich. (1975).
28. G. Arnecke, OPLANT, Unpublished Report, Kernforschungszentrum Karlsruhe (1986).
29. R.E. Kidder, Nuclear Fusion 14, p. 53 - 60 (1974).
30. S. Eliezer, A. Ghatak, H. Hora and E. Teller, An introduction to equations of state: theory and applications, Cambridge University Press, p. 181 (1986).
31. C. Petitjean, private communication (1990).
32. G. Chapline and R. Moir, J. of Fusion Energy, Vol. 5, No. 3, p. 191 - 200 (1986).
33. B. Goel, K. Kufner and W. Höbel, Karlsruhe TARGET CODE, Unpublished Report, Kernforschungszentrum Karlsruhe (1987).

Appendix A - KATACO with Muon Catalyzed Fusion

Additions were made to the one dimensional hydrodynamic lagrangian code KATACO to include simulation of muon catalyzed fusion reactions of deuterium-tritium fuel. KATACO, an updated version of the MEDUSA code, is used to simulate the hydrodynamics and thermodynamics of materials under ion beam or laser irradiation (33). KATACO will also simulate standard deuterium-tritium fusion via it's FUSION subroutine. In the present analysis, KATACO was modified to simulate a 1 cm radius spherical pellet of 50%-50% deuterium-tritium under an external isentropic pressure pulse. The subroutines to calculate the pressure at the pellet surface from ion beam or laser irradiation were short-circuited and a surface pressure history was directly inputted. Once a pressure pulse is inputted and the simulation started, the density is calculated along a radial line of the pellet. The number of meshes along the radial line is selected to provide adequate resolution of the density profile. In this analysis, 50 meshes were used. Each time step the local density of each of the individual meshes is updated using equation state models selected by the user. The ideal gas equation of state was used in this analysis due to it's computational simplicity. In the subroutine FUSION, the energy generated from fusion reactions are calculated. In this subroutine expressions for the energy created and deposited into the fuel due to muon catalyzed fusion of deuterium-tritium were included. The muon catalyzed fusion rate, updated every time step, is calculated using

$$\Delta R = \lambda_c e^{-(\lambda_\mu + \lambda_c w_s) t} N_\mu \Delta t. \quad [\text{EA.1}]$$

The value of λ_c is updated every time step using the expression of the temperature and density dependent μ dt cycling rate in Equation 2.41. The sticking co-efficient w_s is zero in this simulation. The muon catalyzed fusion reaction rate uses the local muon concentration. As the local fuel density in the pellet increases the local muon concentration will also increase. Likewise, as the density decreases the muon concentration decreases. The muon concentration is then simulated using

$$N_\mu(t) = N_\mu(0) \frac{\phi(t)}{\phi(0)} \quad [\text{EA.2}]$$

where N_μ is the muon concentration and ρ is the fuel density. The muon concentration is also updated every time step.

The decay of the muon is taken care of in Equation A.1 by the term λ_μ . With the pressure pulse in Figure 21 inputted and various initial muon concentrations used, the radius of the pellet, the velocity of the pellet's surface, and the fusion energy yields in each case were outputted.